On the generation and degradation of emerged coral reef terrace sequences: first cosmogenic ^{36}Cl analysis at Cape Laundi, Sumba Island (Indonesia)

Denovan Chauveau[a], Christine Authemayou[a], Kevin Pedoja[b], Stéphane Molliex[a], Laurent Husson[c], Denis Scholz[d], Vincent Godard[e], Anne-Morwenn Pastier[f], Gino de Gelder[c], Sri Yudawati Cahyarini[g], Mary Elliot[h], Michael Weber[d], Lucilla Benedetti[e], Marion Jaud[a], Audrey Boissier[i], Vera Christanti Agusta[g], Sonny Aribowo[c], Ann. F. Budd[j], Danny Hilman Natawidjaja[g], A.S.T.E.R. Team[e]

[a]*LGO, IUEM, CNRS, UMR 6538, Université de Bretagne Occidentale, Plouzané, France*
[b]*M2C, UMR6143, UnivCaen-Normandie, Caen, France*
[c]*ISTerre, CNRS, UMR 5275, Université de Grenoble Alpes, Grenoble, France*
[d]*Institut für Geowissenschaften, Johannes-Gutenberg-Universität Mainz, Mainz, Germany*
[e]*CEREGE, CNRS-IRD, UMR 34, Aix-Marseille Université, Aix-en-Provence, France*
[f]*GFZ German Research Centre for Geosciences, Earth Surface Process Modelling, Potsdam, Germany*
[g]*Research Center for Geotechnology, Indonesian Institute of Science, LIPI, Bandung, Indonesia*
[h]*LPG, CNRS, UMR 6112, Université de Nantes, Nantes, France*
[i]*IFREMER, Géosciences Marines, Centre de Brest, Plouzané, France*
[j]*Department of Earth and Environmental Sciences, University of Iowa, Iowa City, USA*

Keywords: Quaternary; Coral reef terrace; ^{36}Cl cosmogenic isotope; Denudation rate; U-Th series; Coastal erosion; MIS 5; Southeastern Asia.

Abbreviations: Coral Reef Terrace (CRT); Marine Isotope Stage (MIS); Electron Spin Resonance (ESR).

Abstract

The emerged coral reef terraces sequence at Cape Laundi, on the north coast of Sumba Island (Indonesia), with at least 18 successive strandlines, remains poorly dated in spite of numerous previous data. The age discrepancies within these coral reef terraces (CRTs) were previously explained by their polycyclic nature, triggered by marine erosion and reoccupation of old coral colonies by new ones. This study aims at highlighting these processes, as well as the continental denudation that participates in the partial stripping of the thin superficial coral reef layer overlying the pre-existing surface, exhuming older coral colonies. For this purpose, we use a combined analysis of ^{36}Cl cosmogenic concentrations, new $^{230}Th/U$ ages, and previous dating in order to quantify denudation rates affecting the sequence and to highlight the role of marine erosion in reworking the lowest CRT surface. Our results demonstrate that 1) the lowermost CRT is composite, i.e., formed by different reefal limestone units constructed and eroded during successive highstands of the last interglacial, 2) following the last deglaciation, this CRT has been subjected again to coastal erosion and reoccupation during the Mid Holocene highstand, 3) its distal edge is affected by the current marine erosion and shows denudation rates higher by one to two orders of magnitude (from 279 ± 0.4 to 581 ± 0.4 mm ka^{-1}) than the continental denudation values of higher CRTs (14.7 ± 8.3 mm ka^{-1} on average), 4) at the scale of a single CRT surface, variations in continental denudation rates are caused by epikarstification roughness, 5) the distal edges have the highest continental denudation rate due to diffusion and regressive erosion produced by the runoff occurring along the steep downward cliff.

1. Introduction

Sumba is an actively rising island in Indonesia where an emerged coral reef terraces sequence records the progressive emergence of the island. The sequence at Cape Laundi, on the north coast of the island, reaches ~470 m in elevation and includes at least 18 successive coral reef terraces (CRTs). This sequence has a well-preserved and potentially valuable record of Quaternary sea level, paleoclimate and tectonics, for which dating of the CRTs is crucial. The previous studies of this CRTs sequence (Pirazzoli et al., 1991; 1993; Bard et al., 1996) have identified significant temporal discrepancies within the CRTs, i.e., different ages of corals within the same CRT and similar ages of corals on several CRTs. Pirazzoli et al. (1991; 1993) and Bard et al. (1996) proposed that the CRTs have a polycyclic nature in order to explain age diachronism (Fig. 1). Pirazzoli et al., (1993) suggested that marine erosion can reshape the CRT surface and promote the bioconstruction of a new coral-colony on an older one during sea level highstands (Fig. 1A). Bard et al. (1996) indicated that a decrease in the rate of uplift to a low rate would in recurrent similar relative sea levels, causing several phases of reef development on a pre-existing surface (Fig. 1B). The role of marine erosion on the morphogenesis of CRTs has been discussed since a long time (e.g., Chappell, 1974; Hearty el al., 2008). Despite the persistence in recent publications of a simplistic definition of CRTs as constructive marine terraces; it is now clearly accepted in many syntheses that a CRT surface results from the combination of bioconstruction, erosion at sea level and accumulation of the eroded sediments (Pirazzoli, 2005; Cabioch, 2011; Murray-Wallace and Woodroffe, 2014; Pedoja et al., 2018; Pastier et al., 2019).

Apart from the role of marine erosion and bioconstruction reoccupation, what is the role of continental denudation in age diachronism on the same CRT? On polycyclic

79 CRT, continental denudation could partially strip the thin superficial layer of a young
80 fossil coral reef and exhume older corals in several places (Fig. 1C). Since the
81 stratigraphy of the CRTs on Sumba is not described and is difficult to observe in the
82 canyons that incise them, and since the preservation of paleo-soils is unlikely in the
83 polycyclic CRTs by their subsequent marine abrasion during a new transgression, we
84 have chosen to combine the cosmogenic ^{36}Cl method (e.g., Lal, 1988; 1991; Bierman,
85 1994), new ^{230}Th/U dating and previous dating to highlight the processes of marine
86 erosion, reoccupation and continental denudation affecting the CRTs of Cape Laundi.
87 The ^{36}Cl method has already been carried out on CRTs in Barbados, resulting in
88 quantification of the continental denudation rate (Lal et al., 2005).
89
90 In this study, we measured the cosmogenic ^{36}Cl isotopes concentration of 34 *in situ*
91 surface samples collected from the oldest CRT to the current reef shelf and took
92 several samples on each CRT from the inner edge to the lower cliff in order to detect
93 variation of continental denudation on them (Figs. 1C; 2). Moreover, we analyzed the
94 ^{36}Cl concentration in a 2.5 ± 0.1 m deep core of the lowermost CRT to attempt to (1)
95 constrain its exposure time to cosmic rays (i.e., the age at which it emerged) if the
96 concentration of ^{36}Cl decreases exponentially at depth (e.g., Braucher et al., 2011), or
97 (2) to detect several exposure phases (i.e., reoccupation stages) by ^{36}Cl concentration
98 peaks at depth (Figs. 1A; 1B). We conducted ^{230}Th/U dating of two coral colonies in
99 growth position collected on the Holocene landform and used these ^{230}Th/U ages to
100 calculate a coastal denudation rate from the ^{36}Cl concentrations of samples taken from
101 the top of the active Holocene sea cliff. We discuss our results in terms of 1) their
102 comparison with global trends, as well as 2) continental denudation rates of carbonates

and their heterogeneity, and 3) the influence of marine erosion and constructive reoccupation components on CRT morphogenesis.

2. Background

2.1. Emerged coral reef terrace sequences

Morphologically, a CRT is an expanse of reefal limestone with a surface that is flat or slightly sloping seawards, limited by a change in slope seaward and landward. Seaward, the change in slope (i.e., a distal edge associated with a more or less steep cliff; Fig. 2), is usually described as the paleo reef crest (e.g., Pirazzoli et al., 1991; Rovere et al., 2016). Landward, at the inner edge, a CRT is characterized by a break in slope, sometimes interpreted as a shoreline angle suggesting the erosional sea cliff nature (e.g., Speed and Cheng, 2004; Pedoja et al., 2018). This break in slope provides a rather good marker for relative sea level, usually associated with the sea level highstands of former interglacial stages (e.g., Pirazzoli et al., 1993; Bard et al., 1996; Pedoja et al., 2018).

CRTs are geomorphologic plane surfaces encountered in the tropical zones and are a type of marine terraces in the broadest sense of the term (Schwartz, 2006; Murray-Wallace and Woodroffe, 2014; Pedoja et al., 2018). When the global sea level falls too rapidly and/or the reef is lifted by tectonic movements or glacial isostatic adjustment, it emerges, dies, and fossilizes, forming a CRT. The joint effects of sea level oscillations and tectonic uplift can result in the generation of a CRTs sequence with a staircase geometry (Fig. 2) (e.g., Chappell, 1974; Pirazzoli, 2005). Since the 19th century, such sequences have been described in the Caribbean province (Haiti, Cuba, Barbados;

e.g., Crosby, 1883; Simms, 2021; Thompson and Creveling, 2021), in the Indo-Pacific province (Indonesia, Papua New Guinea, Japan, Fiji, Philippine, and other islands or archipelagos; e.g., Darwin, 1842; Daly, 1915; Pirazzoli et al, 1993; Pedoja et al, 2018), as well as alongshore the Red Sea (Scholz et al., 2004; Murray-Wallace and Woodroffe, 2014; Pedoja et al., 2011; 2014; Obert et al., 2019).

The stratigraphy and morphology of a CRT, as well as these of a sequence, result from interactions between the vertical land motion, absolute and relative sea level variations, slope of the foundations, erosion processes (either mechanical or chemical and marine or continental in origin), reef bioconstruction, subsequent accumulation of eroded sediments and reef reoccupation (e.g., Pirazzoli, 2005; Cabioch, 2011; Husson et al., 2018; Pedoja et al., 2018; Pastier et al., 2019). Rates of reef growth, marine erosion and sedimentation may vary spatially due to a change in shoreline direction (e.g., from a bay to a cape), resulting in a modification in the final geometry of the sequence (Fig. 2). Thus, one CRT with a continuous high fossil sea cliff (>10 m; CRT I in figure 2) can include numerous secondary or intermediate CRTs (CRTs I_1 and I_2 in figure 2) with or without low (<10 m), eroded, fossil sea cliffs and various reefal limestone units (Fig. 2) (Hantoro et al., 1989; Pirazzoli et al., 1993; Speed and Cheng, 2004). Geomorphologically, these compound CRTs are named main CRTs (e.g., Pirazzoli et al., 1993). These main CRTs, sometimes morphologically forming a single CRT (CRT I in figure 2), may contain coral colonies sampled in growth position on their surface providing ages associated with different Marine Isotope Stage (MIS) (the different reefal limestone units on CRT I in figure 2) (e.g., Pirazzoli et al., 1993; Bard et al., 1996). When such a diachronism is observed, these CRTs are named composite CRTs (e.g., Kindler et al., 2007).

153

154 ## 2.2. Sumba Island

155 ### 2.2.1. Tectonic and geologic setting

156

157 Sumba is a 220 km-long and 65 km-wide island located in the lesser Sunda
158 Archipelago, Indonesia. It is located near the transition from oceanic subduction in the
159 West, along the Java trench, to the collision of the Banda arc with the continental
160 Indian-Australian plate in the East (Fig. 3) (Hinschberger et al., 2005). The Cretaceous
161 to Oligocene crystalline basement is almost entirely covered by Miocene and Pliocene
162 deposits (Abdullah et al., 2000). The Miocene rocks consist of carbonate platform
163 deposits to the west that evolve eastward into deep basin deposits (Von der Borch et
164 al., 1983; Van der Werff et al., 1995). Since the late Miocene/Pliocene, the
165 convergence between the Eurasian and Indian-Australian plates has been driving
166 shortening and uplift in the fore-arc domain (e.g., Harris, 1991; Fortuin et al., 1997;
167 Haig, 2012; Tate et al., 2014). In Sumba island, the Quaternary uplift is recorded by a
168 ~350 km long CRTs sequence (e.g., Pirazzoli et al., 1991; Bard et al., 1996). The
169 Sumba sequence is nearly continuous, interrupted only locally by large rivers. It spans
170 approximately two-thirds of the island's shores, mostly along its northern coast and the
171 eastern and western tips of the island (Hantoro, 1992; Fleury et al., 2009; Nexer et al.,
172 2015; Authemayou et al., 2018).

173

174 ### 2.2.2. Climate and hydrodynamics

175

176 The climate affecting Sumba island is tropical, with humid winters and dry summers,
177 albeit relatively dry compared to other parts of Indonesia (Prasetia et al., 2013). The

mean annual precipitation in Sumba is 1077 ± 406 mm a^{-1} (average over the 1998-2009 period of TRMM data; e.g., Kummerow et al., 2000).

The tides of Sumba Island have a range of ~3.5 m (Colas and Sutherland, 2001; Alfonso-Sosa, 2016; Hibbert et al., 2016). Nevertheless, our study site (Cape Laundi) is located on the northern, leeward side of the island which is only exposed to short wavelength fetch swell (<10 s, i.e., windswell) (Butt et al., 2004).

2.2.3. Previous studies on the Cape Laundi emerged coral reef terraces sequence

Cape Laundi was first mapped by Jouannic et al., (1988). It reaches ~470 m in elevation and has a staircase shape with six main CRTs separated by continuous high (>10 m) fossil sea cliffs (Pirazzoli et al., 1993). Each main CRT includes several intermediate CRTs (Hantoro et al., 1989; Pirazzoli et al., 1993). Marine erosion was detected by Pirazzoli et al. (1991; 1993) from the presence of marine notches in the inner edges of main CRTs, and the observation of coral development surfaces marked by traces of subsequent erosion observed along several canyons transversely cutting the slope of the sequence.

Approximately fifty coral colonies have been dated (using U/Th and ESR dating methods) on the surface of the five lowest main CRTs (T_I to T_{IV1} in Pirazzoli et al., 1993). These ages were correlated to eustatic peaks of the highstands associated, respectively from the oldest to the youngest, to MIS 15 (610 ± 10 ka), MIS 11 (390 ± 30 ka), MIS 9 (325 ± 18.5 ka), MIS 7 (239.5 ± 8.5 ka), MIS 5 (122 ± 6 ka) and MIS 1

(mid Holocene highstand, 6 ± 2 ka) (Pirazzoli et al., 1993; Bard et al., 1996). The oldest dated CRT, named T_{IV1} in previous studies, yielded ESR ages of 584 ± 88 ka and 603 ± 90 ka and was corresponding to MIS 15 (Pirazzoli et al., 1991; 1993). At higher elevations than T_{IV1}, the ages of the successive CRTs were extrapolated assuming a constant uplift rate (i.e., 0.49 ± 0.01 mm a^{-1}; Pirazzoli et al., 1993). The upper, undated CRTs were thus correlated to sea level highstands up to ~1 Ma, i.e., MIS 29 (Jouannic et al., 1988; Pirazzoli et al., 1991; 1993; Hantoro, 1992; Bard et al., 1996).

However, a number of temporal discrepancies emerged with the dating done by Pirazzoli et al. (1991; 1993). Firstly, U-series ages of corals from the same CRT are diachronic (e.g., ages of ~82 ka and ~138 ka from CRT I_1). Secondly, the same U-series ages came from corals on at least three CRTs (e.g., MIS 5e ages on CRTs I_1, I_2, and II_2), and thirdly, U-series ages and ESR ages of corals from the same CRT do not always match with one another. Thereafter, TIMS U-series dating of corals (Bard et al., 1996) specified the diachronism (i.e., MIS 5a, 5c, and 5e ages on CRT I_1; MIS 5c, 5e and pre-MIS 5e ages on CRT I_2).

Bard et al. (1996) interpreted the age inconsistencies to reflect the decrease in uplift rates during a significant period of the late Pleistocene. Very low uplift rates induce negligible uplift of the lowest CRTs before the next transgression, resulting in one or more reoccupation events in which new coral can grow on the pre-existing CRT (Fig. 1B). Combining ^{230}Th/U dating with numerical modeling, Bard et al. (1996) estimated an uplift rate ranging from 0.2 to 0.5 mm a^{-1} and proposed also a polycyclic nature for several CRTs (up to MIS 7). Low uplift rates (0.2 mm a^{-1}) allow coral colonies of a CRT to be recovered by younger ones during a new transgression. But, to obtain the 0.2

mm a^{-1} minimum uplift rate, the previous authors correlated the inner edge of the lowermost main CRT (23 ± 2 m) to MIS 5e, taking into account only the oldest ^{230}Th/U ages. This hypothesis implies that during the MIS 5c and 5a highstands, coastal erosion has been negligible to preserve the morphology of the MIS 5e CRT.

Pirazzoli et al. (1993) interpreted the age inconsistencies to reflect marine erosion. Indeed, they suggested that eustatic sea level fluctuations with efficient marine abrasion superimposed on a regular uplift trend of 0.5 mm a^{-1} must have led sea level to reach nearly the same position several times and the development of bioconstructions differing in age as much as 100 ka on the same CRT (Fig. 1A). The present altitude of dated CRTs allowed Pirazzoli et al. (1991; 1993) to propose an uplift rate trend of 0.49 ± 0.01 mm a^{-1}.

3. Methods

3.1. Mapping, bathymetry, and sampling

3.1.1. Onshore and offshore data

We mapped the inner edges of the CRTs at Cape Laundi using a high resolution (2 m) Digital Elevation Model (DEM) produced from stereoscopic satellite images (Pleaides, CNES) with MicMac freeware (e.g., Rupnik et al., 2016). We acquired topographic and bathymetric profiles, using a real kinematic differential global positioning system (RTK DGPS) onshore, and a Humminbird 700 series sonar offshore (Fig. 4). Onshore, our profiles were carried out perpendicular to the main inner edges of the successive CRTs, parallel to those proposed by Pirazzoli et al. (1993) and starting from the mean

sea level. Profile 1 crosses the whole CRTs sequence and Profile 2 focuses on the lowest CRTs (Fig. 4).

The roughness of the successive CRTs increases with elevation and therefore age because of continental denudation (e.g., epikarst). This roughness is the main source of error in elevation, far beyond instrumental errors. Consequently, we assigned an elevation uncertainty to all the field measurements as a function of the amplitude of the observed natural landform roughness; ± 0.5 m for low standing landforms (<250.5 ± 0.5 m in elevation); ± 1.5 m on the summit of Cape Laundi and the upper CRTs (>250.5 ± 0.5 m in elevation) (Fig. 5).

3.1.2. Sampling strategy

We extracted samples for ^{230}Th/U dating, by drilling two coral colonies in growth positions (samples SUM17-10 and SUM17-13) located on the Holocene CRT (H), near the modern shore (Figs. 3; 4). From the base (CRT H) to the summit of Cape Laundi (CRT VI), we collected 34 samples from the non-vegetated surfaces of the reefal limestones forming the CRTs for cosmogenic ^{36}Cl analysis (Figs. 3; 4). To investigate the potential variability of denudation rates across a given CRT, we collected samples, when possible, from 1) the inner edge, 2) the main surface and 3) the distal edge (Fig. 2).

Below 167.6 ± 0.5 m, intermediate CRTs are distinguishable in the field through fossil sea cliffs (~3 m in height), separated by narrow (80-430 m wide) flat surfaces (Fig. 6). For such CRTs, the distances between two successive sampling sites (i.e., inner edge,

277 main surface, and distal edge) typically range from 20 to 100 m. The CRTs higher than
278 167.6 ± 0.5 m are wider, typically from ~330 to ~1 300 m wide, and our sampling
279 interval is ~500 m.
280
281 To constrain exposure age (i.e., the age at which the CRT emerged), in the case that
282 the concentration of ^{36}Cl decreases exponentially at depth (e.g., Braucher et al., 2011)
283 or to highlight several exposure events (i.e., reoccupation stages), in the case that ^{36}Cl
284 concentration peaks at a certain depth, we drilled the lowermost CRT (I_1) to get a
285 continuous ~2.5 m deep borehole (Fig. 4) (e.g., Braucher et al. 2009; 2011; Hein et al.
286 2009; Schaller et al. 2009). Because of the heterogeneity and porosity of the fossil
287 reefal limestone, our borehole broke into pieces, preventing us from precisely knowing
288 the depths of most of the individual samples. Only the depth of the deepest material
289 recovered from 2.5 ± 0.1 m below the surface of the CRT and the surface sample were
290 considered.
291
292 **3.2. Cosmogenic nuclides**
293
294 The ^{36}Cl cosmogenic concentration in rocks ($N_{(z,t)}$, g^{-1} atom) as a function of depth (z,
295 cm) and time (t, year) can be expressed as follows (Stone et al., 1994):
296
297 $$\frac{\partial N(z,t)}{\partial t} = P(z) - \lambda N(z,t) - \varepsilon \frac{\partial N(z,t)}{\partial z} \quad (1)$$
298
299 z is the depth of a sample. Here, all but one sample (from the bottom of the core in the
300 lowermost CRT) have been collected from exposed bedrock surfaces (z=0), under a
301 surface that denudes at a rate ε (cm a^{-1}). P(z) is the total production rate of ^{36}Cl (atom

302 g^{-1} rock a^{-1}), depending on 1) the cosmic radiation (itself affected by the following
303 parameters: latitude, elevation, topographic shielding, self-shielding (i.e., sample
304 thickness and depth)) passing through a rock of thickness z and 2) on the composition
305 of the rock (Gosse and Phillips, 2001). λ is the decay constant of ^{36}Cl ($\lambda = 2.303.10^{-6}$
306 a^{-1}).
307
308 For all 34 samples, we selected the carbonate matrix containing as few coral fragments
309 as possible. Density measurements on these matrix samples averaged 2.5 g cm^{-3}.
310 Each sample was washed and the fraction 250-1000 µm extracted. About ~100 g of
311 each sample was then used for chemical analysis. We used a standard chlorine
312 extraction protocol, which includes several steps of leaching, designed to remove labile
313 Cl of meteoric origin from mineral surfaces (Stone et al., 1996; Merchel et al., 2008;
314 Schlagenhauf et al., 2010). More precisely, the procedure involved a cleaning process
315 by ultrapure water to remove any suspended particles, followed by a partial dissolution
316 process in 2M HNO_3. Samples were then spiked with ~270 µg of an enriched $^{35}Cl/^{37}Cl$
317 solution in order to determine the ^{35}Cl natural content. Then, the sample was fully
318 dissolved in 2M HNO_3. Residues were filtered from the solution and weighted. 1 ml
319 solution aliquot was collected from the filtered solution for Ca determination. Then, Cl
320 was precipitated as AgCl using $AgNO_3$. The precipitate was dissolved with ammonia
321 and sulfur was reduced by the addition of a saturated $Ba(NO_3)_2$ solution. Afterwards,
322 the solution was filtered and a second precipitation of AgCl was performed with HNO_3.
323 The dried AgCl was finally measured with Accelerator Mass Spectrometry (AMS) at
324 CEREGE (Centre de Recherche et d'Enseignement de Géosciences de
325 l'Environnement) in Aix-en-Provence (France). ^{36}Cl production and denudation rates
326 were calculated following Schimmelpfennig et al. (2009) taking into account Sea-Level-

High-Latitude production rates for rapid neutron spallation reactions (42.2 ± 2 atoms ^{36}Cl (g Ca^{-1} a^{-1}); Braucher et al., 2011; Schimmelpfennig et al., 2011; 2014), negative muons (Heisinger et al., 2002), the rate of epithermal neutron production from fast neutrons (Phillips et al., 2001) and the production from radiogenic neutrons (Fabryka-Martin, 1988; Phillips and Plummer, 1996) (more information related to ^{36}Cl production is detailed in Appendix "A" of Schimmelpfennig et al., 2009). Topographic shielding was calculated for each sample using the topographic shielding add-in for ArcGIS software (Codilean, 2006). The scaling factors are calculated with CosmoCalc 1.7 macro (Vermeesch, 2007; Dunai, 2010). Major oxides (SiO_2, TiO_2, $Al2O_3$, Fe_2O_3, MnO, MgO, CaO, Na_2O, K_2O, P_2O_5) and trace elements (Li, Be, Mo, Ba, Sm, Gd, Pb, Th, U, B, Sc, Cr, Cr, Co, Ni, Rb, Sr) have been measured on the bulk samples (i.e., the size fraction < 250 µm collected after crushing), respectively by an ICP AES-Ultima 2-Jobin Yvon and an HR-ICP-MS Element XR, at the LGO (Laboratoire Géosciences Océan, IUEM) in Brest (France) to determine their impact on the ^{36}Cl production rate. The CO_2 concentration in samples is determined by weighing the samples, dissolving them in a Gas bench and measuring the CO_2 produced (Pôle de Spectrométrie Océan, Plateforme Isotopes Stables, IUEM, Brest, France).

The interaction of secondary cosmic rays with rocks exposed in the Earth's surface produces cosmogenic isotopes (Gosse and Phillips, 2001). Four major interactions are responsible for the production of cosmogenic isotopes, in order of importance: spallation, muon capture, neutron activation, and alpha particle interaction (Bierman, 1994). Except for the production of ^{36}Cl by neutron capture, which peaks at a shallow depth rather than at the surface, cosmogenic isotope production rates decrease exponentially with depth until they stabilize (Stone et al., 1998). The abundance of

cosmogenic isotopes increases with exposure time until steady state, when production and decay of the cosmogenic isotope are balanced (Schlagenhauf et al., 2010). More precisely, when bedrock surfaces are exposed to cosmic ray particles and denuded at a constant rate for long enough, the induced cosmogenic nuclide production equilibrates the losses due to radioactive decay and mass removal linked to denudation processes (Lal, 1991). The cosmogenic nuclide concentration reached at this steady state is inversely proportional to the denudation rate of the surface (e.g., Granger and Riebe, 2014). The time it takes for the concentration of a cosmogenic nuclide to reach steady state depends mainly on the denudation rate. When this steady state is reached, it is possible to quantify the denudation rates without knowing the age of the surface because for any age taken, and for a given ^{36}Cl concentration, the denudation rate will not vary anymore (e.g., Lal et al., 1991; Dunai, 2010). Conversely, for a surface sample that has not reached steady state and was taken on a surface without age constraint, there is an infinite number of age-denudation pair hypotheses that can explain the measured concentration. The denudation rate can be calculated by assuming or independently constraining an exposure age (e.g., using absolute chronological constraints such as ^{230}Th/U ages) and vice versa. Also, constraining both exposure ages and denudation rates when steady state is not reached is possible by fitting a theoretical depth profile, calculated from measured surface and depth concentrations (Braucher et al. 2009; 2011; Hein et al. 2009; Schaller et al. 2009).

In this study, the denudation rates were calculated from ^{36}Cl concentrations assuming a range of absolute ages for CRTs proposed by Pirazzoli et al. (1991; 1993). We show that cosmogenic steady state has been reached for older CRTs than CRT II_7 (corresponding to ~137 m altitude; Fig. 6) because denudation rates remain

unchanged regardless of the chosen age for the CRT. Thus, the age hypotheses are useless to quantify denudation rates for these older CRTs (Section 4.4.). Samples on CRTs surfaces yield continental denudation rates (Fig. 1C), while samples from CRT H yield the quantification of marine erosion (Fig. 1A). Denudation rates are averaged over the time period necessary to erode to a depth equivalent to the neutron characteristic attenuation length (approximately 60 cm in a substrate with a density of 2.5 g cm^{-3}) (Von Blanckenburg, 2005).

3.3. ^{230}Th/U dating

On CRT H (Holocene), at the same sites as the lowest ^{36}Cl samples (SUM18-46 and SUM18-47), we also sampled coral colonies of *Platygyra* (sample SUM17-10) and *Favites* (sample SUM17-13 drilled in a fossil tidal pool) in growth position for ^{230}Th/U dating (Fig. 4). These ^{230}Th/U dating were done on CRT H in order to complete the bibliographic data and to be as close as possible to the cosmogenic nuclide samples to better discuss marine erosion processes. The two samples were mechanically cleaned with a micro-drill and then crushed. Coral samples were rinsed in MilliQ water and leached in 0.1 N bi-distilled HCL for 15-20 minutes in an ultrasonic bath. The cleaned samples were then crushed into powder and analyzed using a XRD Brucker D8 at the LCG (Laboratoire d'étude des "Cycles Géochimiques et Ressources", IFREMER) in Brest (France) to quantify the relative quantities of calcite and aragonite. We proceeded with ^{230}Th/U dating only with two samples, consisting purely of aragonite (>99%).

Subsequently, the powders were dissolved in 7N HNO_3 and a mixed ^{229}Th-^{233}U-^{236}U spike was added to the solution and allowed to equilibrate. A detailed description of the calibration of the spike is given by Gibert et al. (2016). After drying down the solutions, the residues were treated with a mixture of concentrated HNO_3, HCl, and H_2O_2 to remove potential organic components. Then, the solutions were dried again and dissolved in 6N HCl. The fractions of U and Th were then separated from the $CaCO_3$ matrix as described by Yang et al. (2015). For mass spectrometric analysis, the U and Th fractions were dissolved in 2 ml of 0.8N HNO_3. U and Th isotope analysis was performed by multi-collector inductively coupled plasma mass spectrometry at the Institute for Geosciences of the Johannes Gutenberg-University, Mainz (Germany), using a Thermo Fisher Scientific Neptune Plus MC-ICP-MS. A detailed description of the analytical procedures is given by Obert et al. (2016).

4. Results

4.1. Cape Laundi: offshore and onshore landforms

Improved DEM resolution, new bathymetric data and field observations allowed us to improve the mapping of Cape Laundi. The precise description of the coastal morphology is essential to better understand the processes of its formation and destruction. Offshore, two submerged ~200 m wide surfaces (named $-I_1$ and $-I_2$; Fig. 6), were newly identified. Their morphology is consistent with paleo-lagoons: flat in their central part (at -38 ± 1 and -53 ± 1 m for $-I_1$ and $-I_2$, respectively; Fig. 6) and convex at their distal part associated with submerged barrier reefs (at -31 ± 1 and -44 ± 1 m for $-I_1$ and $-I_2$, respectively; Fig. 6). We interpret these bathymetric features as submerged CRTs.

Onshore, seven main CRTs were identified up to 469.8 ± 1.5 m with six major fossil sea cliffs (Figs. 4; 5A; 6). Most of these main CRTs include intermediate CRTs. For example, CRT II, with an inner edge raised at 136.8 ± 0.5 m, is composed of seven intermediate CRTs (II_1, II_2, II_3, II_4, II_5, II_6, II_7) separated by low fossil sea cliffs (<10 m each). The lowermost main CRT (CRT I) is 550 m wide, has an inner edge raised at 23.2 ± 0.5 m, and includes of two intermediate CRTs (I_1, I_2) separated at 6.4 ± 0.5 m by a ~3 m high fossil sea cliff. On profile 2, CRT I is only 200 m wide, its surface is irregular, and the two intermediate CRTs (I_1, I_2) are separated at 7.6 ± 0.5 m by a ~15 m high fossil sea cliff.

CRT I1 consists of well-preserved smooth flat surfaces (Figs. 5C; 5D). In places, its surface is covered by centimeter-scale remnants of a sandstone layer including coral rubbles (Fig. 5E). The surface of CRT I_2 is irregular and exhibits some isolated smooth multi-centimetric carbonate surfaces attesting for the relatively quick formation of rough surfaces on the CRT. This superficial layer becomes rougher and thicker from CRT II_2, where it reaches ~20 cm (Fig. 5B). At the highest CRTs, epikarstic roughness reaches 1 to 2 m (Figs. 5F; 5G). Moreover, the roughness varies across the CRTs, between ~0.1 to ~2 m, i.e., the inner edges and the main surfaces of the CRTs are rather smooth whereas their distal edges are rougher (Fig. 5G).

Alongshore, Holocene landforms are represented by a conglomerate, remnants of limestone banks of fossil reef, and coral colonies in growth position, reaching approximately 2 ± 0.5 m above mean sea level (Fig. 5C). Remnants of CRT H have a restricted width (~5 m) and are delimited seaward by active sea cliffs (Fig. 5C). On the

flat surface of CRT H, some fossil corals appear very well-preserved and most frequently located in circular depressions with their associated ramparts filled by a white and fresh carbonated matrix (Fig. 5I). The diameter of such circular landforms is generally ~1 m and we interpret them as fossil tidal pools (Fig. 5I) (Hoeksema, 2012). Fossil coral colonies samples within this Holocene emergent reef have been previously cross-dated from 2.03 ± 0.18 to 6.32 ± 0.14 (Jouannic et al., 1988; Pirazzoli et al., 1991, 1993; Bard et al., 1996). The modern reef flat (called I_0 on Fig. 5B) is typical of a fringing reef, as previously interpreted by Bard et al. (1996). There are living corals on the reef crest (seaward), whereas landwards the reefal flat is covered by coral rubbles (Fig. 5J) and associated with beaches and/or mangroves at some sites.

4.2. ^{230}Th/U dating of the Holocene CRT

The two fossil coral samples display ^{238}U concentrations between 2.4 and 3 ppm (Table 1). Low ^{232}Th contents together with high (^{230}Th/^{232}Th) activity ratios argue for a lack of significant detrital contamination. Both samples display initial δ^{234}U values that agree within errors with a mean modern ocean water value of δ^{234}U = 146.8 ± 0.1‰ (Andersen et al., 2010), indicating closed system evolution and no evidence for diagenetic alteration. These coral colonies samples yielded ^{230}Th/U ages of 5.45 ± 0.02 ka (sample SUM17-10) and 2.13 ± 0.01 ka (sample SUM17-13) (Table 1).

4.3. Distribution of ^{36}Cl concentration at the scale of the emerged coral reef terraces sequence

The ^{36}Cl concentrations obtained from the samples along profiles 1 and 2 range from 3.68 ± 0.08 to 20.00 ± 0.37.10^5 atoms g^{-1} rock and average at 7.74 ± 3.67.10^5 atoms g^{-1} rock (n = 28; Table 2). Given the overall uniform lithology and precipitation rate, the variability across the profile is higher than expected if all measured ^{36}Cl concentrations have been controlled by steady erosion. The six measured ^{36}Cl concentrations of samples from CRT I have low variability (with an average at 5.54 ± 0.67.10^5 atoms g^{-1} rock) compared to the ^{36}Cl concentration of all other/older samples (with an average at 8.25 ± 3.90.10^5 atoms g^{-1} rock). The ^{36}Cl concentration measured at the base (sample SUM18-47: 0.30 ± 0.05.10^5 atoms g^{-1} rock) and on the top of the modern sea cliff (sample SUM18-46: 0.38 ± 0.08.10^5 atoms g^{-1} rock) are an order of magnitude lower than those measured on Pleistocene CRTs (I-VII) (Table 2). At the borehole site (Fig. 4), the ^{36}Cl concentrations measured at the surface ($Cm_{surface}$) and at a depth of 2.5 ± 0.1 m ($Cm_{2.5m}$) are 6.23 ± 0.28 and 2.46 ± 0.12.10^5 atoms g^{-1} rock, respectively (Table 2).

4.4. Denudation rates

The time scales over which denudation rates are integrated (Von Blanckenburg, 2005) range from 16.2 ± 0.3 (highest rate) to 237.3 ± 27.0 ka (lowest rate) with an average of 61.7 ± 49.6 ka (n = 66). Denudation rates for the various CRTs of the sequence range from 2.5 ± 0.1 to 37.1 ± 0.9 mm ka^{-1} (average at 14.7 ± 8.3 mm ka^{-1}, n = 66) (Table 3; Fig. 6). Despite the different age hypotheses for CRT I, the denudation rates calculated are more uniform than those determined for the upper CRTs (Table 3; Fig. 6). Denudation rates from the CRTs II_2, II_3, and II_4 are rather similar, irrespective of different age hypotheses (Table 3; Fig. 6). The results suggest that cosmogenic steady

state has been reached for older CRTs than II_7; i.e., whatever the assigned age to the CRT, the calculated denudation rates for these CRTs do not vary much (Table 3; Fig. 6).

The average denudation rates affecting the inner edges, main surfaces and distal edges of the CRTs are 11.1 ± 7.0 (n = 16), 14.3 ± 6.8 (n = 38), and 20.8 ± 8.6 mm ka^{-1} (n = 12) respectively. Denudation rates for CRTs main surfaces are widely dispersed and range from 2.5 ± 0.3 (sample SUM18-37) to 29.4 ± 1.4 mm ka^{-1} (sample SUM16-8). Apart from the denudation rate calculated for sample SUM18-15 (Table 3), denudation rates affecting the inner edges of CRTs I_1, II_1, II_4, II_6, V, VI are similar to those of the fossil reef flats. Denudation rates for the distal edge of the CRTs are higher than rates from other parts of the landform. Since the number of denudation rate values is low, a non-parametric statistical test was performed (Kruskal-Wallis test) to determine whether denudation rates vary significantly by morphological location of the samples analyzed. The average rank of the calculated denudation rates is not statistically significantly different according to the morphological location of the samples (P_{value} = 0.26). Thus, the morphology of the CRTs does not fully explain the heterogeneity of the calculated denudation rates.

Sample SUM18-46 was collected from the same surface (CRT H) of the samples used for ^{230}Th/U dating (SUM17-10 and SUM17-13) (Figs. 4; 5C). Considering ^{230}Th/U ages as the exposure time of the surface, we calculated denudation rates of 279.0 ± 0.4 mm ka^{-1} and 581.0 ± 0.4 mm ka^{-1} (Table 3). These denudation rates (average of 430 ± 214 mm ka^{-1}; Table 3) near the sea level are much higher, by one to two orders of magnitude, than the denudation rates calculated for the other CRTs (I-VI).

5. Discussion

Significant denudation rates obtained at the sea level and on the CRTs sequence point to marine erosion and continental denudation as the cause of the age diachronism on a single CRT (Figs. 1A; 1B). This hypothesis also requires reef reoccupation over several highstands (R2 over R1 on figure 1). Our results provide the opportunity to discuss the dynamics of these processes at Cape Laundi. We first highlight the role of reef reoccupation processes and marine erosion in shaping CRTs. Then, we discuss continental denudation by comparing our data with denudation rates published for the Barbados and Puerto Rico CRTs (Lal et al., 2005), as well as for other carbonate landscapes (e.g., Spencer, 1985; Vasconcelos and Stone, 2000), and focusing on the variability of denudation rates.

5.1. The genesis of the lowermost main CRT (I)

5.1.1. Reefal limestone units overlapping

Whatever the hypothesis to explain diachronous ages on the same CRT surface, the CRT internal architecture must be associated with a phenomenon of reef reoccupation over several highstands in order to have recent thin reef units stacked on older units (R2 over R1 in figure 1). In the borehole site of CRT 1, theoretically, if both measured samples belong to the same reefal limestone unit, the ^{36}Cl concentration profile in depth (constrained by an erosion rate and age) should decrease exponentially and join the two measured ^{36}Cl concentration points. To construct this profile, we (1) made different age hypotheses for CRT I_1, (2) used the ^{36}Cl concentration measured at the

surface ($Cm_{surface}$) to start the profile, (3) set the denudation rate automatically by combining the measured ^{36}Cl concentration at the surface ($Cm_{surface}$) with the chosen hypothetical age, and (4) set a minimum and a maximum of reef porosity from 0% (i.e., density 2.5 g cm^{-3}) to 50 % (i.e., a density of 1.25 g cm^{-3}) (e.g., Smith, 1983). We test the ages proposed by Pirazzoli et al. (1991; 1993): MIS 5e, c and a, as well as an extremely old age, i.e., 1.5 Ma, to test a steady state hypothesis (Schimmelpfennig et al., 2009).

In any case, it is not possible to join the two ^{36}Cl concentrations measured by the theoretical ^{36}Cl concentration profiles (Fig. 7). Regardless of the scenario, the 2.5 ± 0.1 m deep sample exhibits a ^{36}Cl concentration higher than its theoretical estimate (Fig. 7). The only exception is observed with a 50% porosity and the age of the drilled unit estimated at 1.5 Ma. However, this age is too old compared to the dating done by previous authors on the studied CRT (Pirazzoli et al., 1991; 1993; Bard et al., 1996). The only way to explain the high ^{36}Cl concentration of the sample at 2.5 ± 0.1 m is that this reefal limestone unit has been exposed to cosmic radiation before an overlapping unit was emplaced, i.e., in a later stage of reoccupation. It follows that the borehole goes through two reefal limestone units, the upper one being thinner than 2.5 m.

We thus hypothesize that this difference in the ^{36}Cl concentrations measured has been acquired on the temporarily emerged surface of the CRT between two successive highstands. We then calculate exposure times before overlapping with Δc (i.e., difference between the measured and theoretical ^{36}Cl concentration at a depth of 2.5 m; Table 4) according to possible ages of MIS 5a, MIS 5c and MIS 5e for the surface unit ($Ed_{\Delta c}$ in Table 4; Pirazzoli et al., 1991; 1993; Bard et al., 1996). These values

575 correspond to minimum exposure time because after overlapping, the ^{36}Cl
576 concentration decreases with isotopic decay. Considering the ages of MIS 5e, 5c and
577 5a, which are 122 ± 6 ka, 100 ± 5 ka, and 82 ± 3 ka, respectively (Cutler et al., 2003),
578 the time intervals between isotopic stages 5e-5c, 5c-5a and 5e-5a are 22 ± 11 ka, 18
579 ± 8 ka, and 40 ± 9 ka, respectively. For the zero-porosity hypothesis, the calculated
580 exposure times before overlapping (13.8 ± 1.3 ka, 12.5 ± 1.2 ka, and 11.0 ± 1.2 ka) are
581 equivalent to the time intervals between two successive substages of MIS 5 (Table 4).
582 Consequently, our data argue that the borehole intersected two units that could be
583 associated to the two of the three relative highstands of the last interglacial: MIS 5a
584 and 5c, or MIS 5c and 5e (Table 4; Fig. 7).
585
586 We conclude that the ^{36}Cl borehole method confirms previous observations deduced
587 from $^{230}Th/U$ ages (Pirazzoli et al., 1991; 1993; Bard et al., 1996), and that CRT I_1 is
588 composite and was built during at least two successive highstands of the last
589 interglacial.
590
591 **5.1.2. Evidence for marine erosion and constructive reoccupation**
592
593 Combining comosgenic nuclide analyses and $^{230}Th/U$ dating on reef samples collected
594 near sea level allows to discuss the hypothesis of Pirazzoli et al., (1993) that reef
595 reoccupation is associated with marine erosion (Fig. 1A). Our two samples from CRT
596 H, one at the base (SUM18-47, 0.30 ± 0.03.10^5 atoms g^{-1} rock) and the other at the
597 top of the modern sea cliff (SUM18-46, 0.38 ± 0.04.10^5 atoms g^{-1} rock), give similar
598 low ^{36}Cl concentrations (Table 2). If sample SUM18-47 had been recently exposed by
599 sea cliff retreat, its ^{36}Cl concentration would be much lower (e.g., Regard et al., 2012).

Therefore, the two samples at the top and the base of the modern sea cliff likely experienced the same erosive history over the time interval resolved by the ^{36}Cl method (~1.5 ka). In view of their location close to sea level and the high denudation rates calculated from the top of the modern sea cliff (average of 430 ± 214 mm ka^{-1}), the erosion process is most likely marine. The efficiency of marine erosion has already been demonstrated by numerous studies, in particular using cosmonuclides (Gibb, 1978; Spencer, 1985; Stephenson and Kirk, 1998; Brown et al., 2003; Raimbault et al., 2018). In Grand Cayman Island, the average marine erosion rate affecting reef shielded coasts is 450 mm ka^{-1} (Spencer, 1985), which is in agreement with our denudation rate values. However, denudation rates affecting the active sea cliff at Cape Laundi were calculated on small length (sample of few centimeters) and time (age hypothesis of few thousand years) scales. It may reflect the stochastic nature of erosion, i.e., the detachment of a small block that can generate a large difference on the calculated denudation rates. Such efficient erosion at sea level during a relatively short period of time can be caused by extreme events, such as storms, cyclones, or tsunamis (Anderson et al., 1999). Consequently, a comparison with denudation rates averaged over much larger temporal and spatial scales may be misleading.

Whatever the uplift rate or the value of the glacial isostatic adjustment, the location of the samples dated at 5.45 ± 0.02 ka and 2.13 ± 0.01 ka at the same altitude and a few metres apart can only be explained by erosion and reoccupation. In addition, we have observed fossil tidal pools on the CRT H surface (Fig. 5I), where the coral dated as 2.13 ± 0.01 ka was sampled, which allows us to specify the reoccupation mode. Therefore, we interpret the coral dated at 2.13 ± 0.01 ka (SUM17-13) as a coral-colony that settled on the top surface of the active sea cliff in fossil tidal pools fed by seawater

during high tides or storms, as observed elsewhere (e.g., Hoeksema, 2012). As such, we conclude that the constructive reoccupation affected the CRT H during the Mid-Holocene with a partial immersion of the reef platform.

5.1.3. Argument of the abandonment of the main CRT (I) in a single eustatic event.

Cosmogenic nuclide data also inform us about the processes of CRT abandonment during regression. CRT I is not old enough to have reached cosmogenic steady state. However, ^{36}Cl concentrations measured on the main CRT I (I_1, I_2) are uniform (Table 2, Fig. 6), suggesting a similar exposure time to radiation for the whole surface of CRT I. Thus, the abandonment of CRT I surface most probably corresponds to a discrete, single event, during regression after the last interglacial highstand.

5.2. Continental denudation of CRTs

5.2.1. Comparison with global trends of carbonate denudation rates

In previous studies, continental denudation of reef carbonate landforms has been quantified by taking direct *in situ* measurements, for example, ^{36}Cl concentrations (Lal et al., 2005) as well as micro-erosion (e.g., Trudgill, 1976; 1979). Each method is representative of a given period of time on which the calculated denudation rates are integrated. For the ^{36}Cl method, this period is between 10^3 to 10^5 years. In contrast, the micro-erosion method covers periods of only one to two years (e.g., Trudgill, 1976; Spencer, 1985).

Denudation rates at Cap Laundi (average of 14.7 ± 8.3 mm ka^{-1}), where precipitation rates are ~1000 mm a^{-1}, are lower than those of tropical sites with higher rainfall (> 2000 mm a^{-1}), such as in Papua New Guinea (denudation rate of ~150 mm ka^{-1}, Vasconcelos and Stone, 2000), higher than those obtained in arid to hyper-arid zones (denudation rate of from 1 to 3 mm ka^{-1}, Ryb et al., 2014) and similar to those derived with the same method (^{36}Cl concentration) on the same features (upper Pleistocene CRTs) at locations with the same mean annual precipitation rates (1200-1500 mm a^{-1} in Rendezvous Hill, Barbados and ~915 mm a^{-1} in Isla Mona, Puerto Rico). Denudation rates range from 7 to 118 mm ka^{-1} on the Rendezvous Hill and from 26 to 61 mm ka^{-1} at Isla Mona (Lal et al., 2005). Trudgill (1976; 1979) obtained similar denudation rates (9-62 mm ka^{-1}) in Aldabra atoll (Seychelles archipelago), that receives comparable rainfalls (Shekeine et al., 2015). Thus, denudation rates calculated at Cape Laundi are consistent with the global correlation between rainfall and denudation rates determined by the *in situ* ^{36}Cl method on carbonate flat surfaces (Ryb et al., 2014; Levenson et al., 2017). These continental denudation rates imply a surface stripping rate of 0.7 to 2.3 m per glacial/interglacial cycle. If the younger reef unit are thin as suggested by the drilling results, this stripping is sufficient to reveal older reef units at the surface (Fig. 1C).

5.2.2. Heterogeneous variations of denudation rates across the sequence as well as individual CRT

Denudation rates (i.e., ^{36}Cl concentrations) vary across the sequence, as well as within each CRT. In the following, we propose that this is mainly due to the sampling bias

675 related to the roughness of the carbonate surfaces and the staircase morphology of
676 the sequence.
677
678 **5.2.2.1. Roughness versus ^{36}Cl concentrations**
679
680 Over time, aerial dissolution forms larger and larger dissolution pits, amplifying the
681 roughness of the CRT (Figs. 5A; 5B; 5F; 5G). Thus, at Cape Laundi, the older the CRT,
682 the rougher it is (Figs. 5A; 5B; 5F; 5G). The roughness of all CRTs is in the order of
683 decimeters (Fig. 5B). We also observed a coastal karren-type epikarstification (e.g.,
684 Lundberg, 2019). This process induces a detachment of 10 to 50 cm thick blocks from
685 the CRT surface (Figs. 5B; 8A; 8B). The types of corals, sediments, and stage of
686 cementation produce distinctive layers of limestone rocks in fossilized reefs (James
687 and Macintyre, 1985). The layering of the paleo-reef could therefore play an important
688 role in the development of these karstic forms (Figs. 8A; 8B).
689
690 Block detachment could produce a change of ^{36}Cl concentrations over the CRTs
691 surfaces with low values on recently dismantled zones. The following goal is to get an
692 independent estimate of the typical block size removed by these karstification
693 processes using our ^{36}Cl data. We selected two pairs of surface samples from the flat
694 part of the same CRT that yield different ^{36}Cl concentrations (SUM18-21/SUM16-4 and
695 SUM18-20/SUM16-10) and we hypothesized that the difference in ^{36}Cl concentration
696 values for each pair is related to the dismantling of the surface blocks. The pairs are
697 located on CRTs I_2 and II_4, respectively (Fig. 8C). We calculate the theoretical depth
698 profile of ^{36}Cl concentrations from the CRTs age inferred by Pirazzoli et al. (1991; 1993)
699 combined with the measured ^{36}Cl concentration for the most concentrated surface

sample (Fig. 8C). To quantify the stripped thickness required to achieve the lowest ^{36}Cl concentration of each pair, we projected this concentration onto the calculated theoretical depth profile of ^{36}Cl concentrations (Fig. 8C). We obtained stripped thicknesses of ~30 cm and ~82 cm for CRTs I_2 and II_4, respectively (Fig. 8C). These results are consistent with the natural roughness observed and the height generated by the detachment of a block (Figs. 5B; 8A). Thus, the difference in ^{36}Cl concentration between each pair of samples can be attributed to the removal of a single block. Variations in ^{36}Cl concentration on the same CRT can be explained by the spatial variations of the degradation of the initial CRT surface. The greater the thickness of the removed blocks, the greater the variations in ^{36}Cl concentration at the surface related to its dismantling will be (Figs. 8B; 8C). Such spatial variations in denudation rates imply that it is impossible to accurately date, with the analysis cosmogenic ^{36}Cl concentrations, a CRT that has not yet reached the steady state (such as CRT I) because it requires having a uniform value of this parameter all along the CRT. Besides, these results suggest that on a given polycyclic CRT, the continental denudation can partially strip the thin superficial layer of a young fossil coral reef and exhume older corals in several places.

5.2.2.2. CRT morphology versus ^{36}Cl concentrations

When samples are divided according to their distribution on the CRT (i.e., inner edge, terrace main surface, and distal edge) (Table 3), denudation rates reveal different averages, with the highest values for the distal edges (Fig. 9). Although the non-parametric statistical test (Kruskal-Wallis test) reveals that there is no significant difference in denudation rates as a function of the morphological location of the sample

analyzed (P_{value} = 0.26), we consider that the distal edges are the most sensitive to continental denudation because of their position at the top of the slope (Figs. 2; 6). In this case, distal edges could be faster dissolved by diffusion between the fossil sea cliff and fossil reef flat, and regressive erosion associated with runoff on the cliff. The flat geometry of the CRT main surfaces prevents diffusion and runoff that could increase the denudation rate. Furthermore, there may be a change in porosity between the main surface and the distal edge of CRTs that may cause the dissolution rate to vary spatially. The main surfaces of CRTs, considered a paleo lagoon (Cabioch, 2011), can be then partly formed by the compaction and deposition of marine cements (Figs. 5C; 5D; 5E; Hopley, 2011), which reduces the porosity of the framework. The distal edges of the CRTs, considered as the paleo reef crests (e.g., Pirazzoli et al., 1991; Rovere et al., 2016), therefore appear to have a higher porosity than the main surfaces. The greater the porosity, the more it allows the infiltration of meteoric water, accelerating chemical dissolution and therefore potentially the denudation rate. Which in turn explains the high roughness of the distal edges compared to other parts of the CRTs (Fig. 5G).

5.2.2.3. Water, sands cover and soil formation on CRT versus ^{36}Cl concentration

CRTs may be flooded during the subsequent interglacial substages if uplift rates are low or if marine erosion lowers the CRT (Fig. 1). This process could play a role in shielding and affect the production of ^{36}Cl on CRTs older than Holocene. However, the integration time of the denudation rates calculated here (i.e., 61.7 ± 49.6 ka in average) is too short to have recorded several highstands.

Besides, CRTs may also be covered by sand and debris during and after periods of intense marine erosion. Indeed, we observed that CRT I_1 surface is covered by centimeter-scale remnants of a sandstone layer including coral rubbles (Fig. 5E). The process that forms this layer may be related to marine diagenetic cementation (Rasser and Riegl, 2002). Storms are the natural events that generally explain the formation and deposition of these layers (e.g., Scoffin, 1993; Bourrouilh-Le Jan, 1998; Blanchon et al. 1997; Rasser and Riegl, 2002). Yet, they are also common features in sites characterised by gently sloping, pre-existing surfaces (i.e., composite CRTs in our study site) and medium wave energy (Cabioch et al., 1995). These sand patches are widely scattered on the lower CRTs and are absent on the upper CRTs due to continental denudation. They must have been removed during the CRT emergence by marine erosion (only a few pieces remain; Figs. 5C; 5E) and by continental denudation after the reef emersion. With a continental denudation rate of 14.7 ± 8.3 mm ka^{-1} on average, it takes only ~7000 years to strip off a few tens of centimeters. Besides, this thickness is too small to significantly affect the denudation rates and to be distinguished from the stripping effect.

Our field observations have shown that soil is almost non-existent on the lowest CRTs (Figs. 5D; 5E) and the soil on CRTs above CRT III is very thin (a few millimeters to centimeters) and only allows the formation of vegetation of steppe moor (Figs. 5A; 5B; 5D; 5F; 5G). The relatively dry climate of the Cape Laundi region (e.g., Prasetia et al., 2013) may be the cause of the lack of thick soil, which can affect the production of ^{36}Cl. But despite this arid climate, the contribution of volcanic ash from the Sunda-Banda arc or of Australian dust could favour the development of soil. This has already been

observed in Barbados, where the parent materials of the soils on uplifted CRTs are Sahara dust and volcanic ash from the Lesser Antilles Island arc (Muhs, 2001). Similar examples have been reported in Taiwan (Liew and Hsieh, 2000) as well as in Liuchiu Island (Cheng et al., 2011). It remains an open question whether deforestation (e.g., Orr et al, 2012) and agricultural burning (e.g., Russell-Smith et al., 2007) could have removed the soil formed over time, despite the low runoff induced by the horizontality of the surfaces of the CRT. We have not observed any soil trapped and preserved in the dissolution features (i.e., coastal karren; Lundberg, 2019) or superficial cracks of the CRTs to testify to its previous existence. Over time, soil forms from the *in situ* weathering of the initial surface of the CRT and thickens. An older CRT should therefore have a thicker soil, a more weathered surface and be more protected from cosmic rays (shielding action) than a more recent CRT. Thus, we should have observed a decrease in the ^{36}Cl concentration with the age of the CRT with former thick soil now gone. We have not observed such a trend in our data. Therefore, we have no evidence of the influence of soils on the ^{36}Cl production in the CRTs at Cape Laundi.

6. Conclusions

At Cape Laundi, previous studies (Pirazzoli et al., 1991; 1993; Bard et al., 1996) have identified age discrepancies on CRTs. We disentangled the roles of continental denudation, coastal erosion, and marine reoccupation in the promiscuity of diachron coral colonies on the same CRT surface. The ^{36}Cl concentrations of 34 surface limestone samples taken from different morphological zones of this CRTs sequence allowed us to calculate continental denudation rates, ranging from 2.5 ± 0.3 to 37.1 ±

800 0.1 mm ka^{-1} (14.7 ± 8.3 mm ka^{-1} on average). The combined analysis of $^{230}Th/U$ ages
801 and cosmogenic ^{36}Cl concentrations of surface and depth samples in both the distal
802 and proximal part of the lowermost CRT suggest that this CRT is composite and
803 records a polycyclic history with alternating construction and erosion phases during the
804 eustatic sea level variations of the last interglacial highstands (MIS 5e, 5c, and 5a) and
805 during the Mid-Holocene. Our results also highlight 1) significant spatial variability in
806 denudation rates, probably related to roughness and morphological zoning of CRTs,
807 which could bring coral colonies of different ages to the surface depending on the
808 efficiency of continental denudation, and 2) higher denudation rates affecting the distal
809 edges of CRTs than in other parts of the landform. Eventually, we stress that such
810 erosion processes, suggested since a long time but rarely discussed in the literature,
811 should be systematically taken into account when establishing the morphostratigraphy
812 of emerged coral reef terrace sequences.
813
814 **Acknowledgements**
815
816 This work was supported by public funds received in the framework of GEOSUD, a
817 project (ANR-10-EQPX-20 and ANR-10-LABX-19-01, Labex Mer, CLIMORESO, C.
818 Authemayou) of the program "Investissements d'Avenir" managed by the French
819 National Research Agency, the INSU Tellus Syter program (SECOMAS, C.
820 Authemayou) and the CNES TOSCA program (CETTROPICO, C. Authemayou). We
821 thank the German Aerospace Center for providing us the TanDEM-X data for our study
822 zone. We thank the State Ministry of Research and Technology of Indonesia “RISTEK”
823 that allowed us to conduct the field trip to Sumba (research permit
824 680/FRP/E5/Dit.KI/IV/2017). We also thank the National Geographic Explorer grant

(no CP 087R 17) to support the Indonesian researchers (Sri Yudawati Cahyarini, Vera Christanti Agusta, and Danny Hilman Natawidjaja). Denis Scholz is thankful to the DFG for funding (SCHO 1274/11-1 and INST 247/889-1 FUGG). We thank Gilles Brocard for his help with karstic terminology. Finally, we thank 3 anonymous reviewers for fruitful discussions on former versions of this manuscript.

References cited

1. Abdullah, C. I., Rampnoux, J. P., Bellon, H., Maury, R. C., & Soeria-Atmadja, R. (**2000**). The evolution of Sumba Island (Indonesia) revisited in the light of new data on the geochronology and geochemistry of the magmatic rocks. Journal of Asian Earth Sciences, 18(5), 533-546.

2. Alfonso-Sosa, E. (**2016**). Tidal mixing in the Sumba Strait and internal wave activity detected during strong semidiurnal forcing.

3. Andersen, M. B., Stirling, C. H., Zimmermann, B., & Halliday, A. N. (**2010**). Precise determination of the open ocean 234U/238U composition. Geochemistry, Geophysics, Geosystems, 11(12).

4. Anderson, R. S., Densmore, A. L., & Ellis, M. A. (**1999**). The generation and degradation of marine terraces. Basin Research, 11(1), 7-20.

5. Authemayou, C., Brocard, G., Delcaillau, B., Molliex, S. p., Pedoja, K., Husson, L., et al. (**2018**). Unraveling the roles of asymmetric uplift, normal faulting and

groundwater flow to drainage rearrangement in an emerging karstic landscape. Earth Surface Processes and Landforms, 43(9), 1885-1898.

6. Bard, E., Jouannic, C., Hamelin, B., Pirazzoli, P., Arnold, M., Faure, G., et al. (**1996**). Pleistocene sea levels and tectonic uplift based on dating of corals from Sumba Island, Indonesia. Geophysical Research Letters, 23(12), 1473-1476.

7. Bierman, P. R. (**1994**). Using in situ produced cosmogenic isotopes to estimate rates of landscape evolution: A review from the geomorphic perspective. Journal of Geophysical Research: Solid Earth, 99(B7), 13885-13896.

8. Blanchon, P., Jones, B., & Kalbfleisch, W. (**1997**). Anatomy of a fringing reef around Grand Cayman; storm rubble, not coral framework. Journal of Sedimentary Research, 67(1), 1-16.

9. Bourrouilh-Le Jan, F. G. (**1998**). The role of high-energy events (hurricanes and/or tsunamis) in the sedimentation, diagenesis and karst initiation of tropical shallow water carbonate platforms and atolls. Sedimentary Geology, 118(1-4), 3-36.

10. Braucher, R., Del Castillo, P., Siame, L., Hidy, A. J., & Bourles, D. L. (**2009**). Determination of both exposure time and denudation rate from an in situ-produced 10Be depth profile: a mathematical proof of uniqueness. Model sensitivity and applications to natural cases. Quaternary Geochronology, 4(1), 56-67.

11. Braucher, R., Merchel, S., Borgomano, J., & Bourlès, D. L. (**2011**). Production of cosmogenic radionuclides at great depth: a multi element approach. Earth and Planetary Science Letters, 309(1-2), 1-9.

12. Brown, J., Jorgenson, M. T., Smith, O. P., & Lee, W. (**2003**). Long-term rates of coastal erosion and carbon input, Elson Lagoon, Barrow, Alaska. Paper presented at the Eighth International Conference on Permafrost.

13. Butt, T., Russell, P., & Grigg, R. (**2004**). Surf science: An introduction to waves for surfing: University of Hawaii Press Honolulu.

14. Cabioch, G., Montaggioni, L. F., & Faure, G. (**1995**). Holocene initiation and development of New Caledonian fringing reefs, SW Pacific. Coral Reefs, 14(3), 131-140.

15. Cabioch, G. (**2011**). Emerged reefs. Encyclopedia of Modern Coral Reefs: Structure, Form and Process, 373-380.

16. Chappell, J. (**1974**). Geology of coral terraces, Huon Peninsula, New Guinea: a study of Quaternary tectonic movements and sea-level changes. Geological Society of America Bulletin, 85(4), 553-570.

17. Cheng, C.-H., Jien, S.-H., Tsai, H., & Hseu, Z.-Y. (**2011**). Geomorphological and paleoclimatic implications of soil development from siliceous materials on the

coral-reef terraces of Liuchiu Island in southern Taiwan. Soil science and plant nutrition, 57(1), 114-127.

18. Codilean, A. T. (**2006**). Calculation of the cosmogenic nuclide production topographic shielding scaling factor for large areas using DEMs. Earth Surface Processes and Landforms, 31(6), 785-794.

19. Colas, A., & Sutherland, B. (**2001**). The world stormrider guide: Low Pressure.

20. Crosby, W. O. (**1883**). Elevated coral reefs of cuba. Journal of Natural History, 12(70), 283-284.

21. Cutler, K. B., Edwards, R. L., Taylor, F. W., Cheng, H., Adkins, J., Gallup, C. D., et al. (**2003**). Rapid sea-level fall and deep-ocean temperature change since the last interglacial period. Earth and Planetary Science Letters, 206(3-4), 253-271.

22. Daly, R. A. (**1915**). The glacial-control theory of coral reefs.

23. Darwin, C. (**1842**). The Structure and Distribution of Coral Reefs: Being the First Part of the Geology of the Voyage of the Beagle... During the Years 1832-1836: Smith, Elder.

24. Dunai, T. J. (**2010**). Cosmogenic Nuclides: Principles, concepts and applications in the Earth surface sciences: Cambridge University Press.

25. Fabryka-Martin, J. T. (**1988**). Production of radionuclides in the earth and their hydrogeologic significance, with emphasis on chlorine-36 and iodine-129.

26. Fleury, J.-M., Pubellier, M., & de Urreiztieta, M. (**2009**). Structural expression of forearc crust uplift due to subducting asperity. Lithos, 113(1-2), 318-330.

27. Fortuin, A. R., Van der Werff, W., & Wensink, H. (**1997**). Neogene basin history and paleomagnetism of a rifted and inverted forearc region, on-and offshore Sumba, Eastern Indonesia. Journal of Asian Earth Sciences, 15(1), 61-88.

28. Granger, D. E., & Riebe, C. S. (**2014**). Cosmogenic nuclides in weathering and erosion.

29. Gibb, J. G. (**1978**). Rates of coastal erosion and accretion in New Zealand. New Zealand journal of marine and freshwater research, 12(4), 429-456.

30. Gosse, J. C., & Phillips, F. M. (**2001**). Terrestrial in situ cosmogenic nuclides: theory and application. Quaternary Science Reviews, 20(14), 1475-1560.

31. Haig, D. W. (**2012**). Palaeobathymetric gradients across Timor during 5.7-3.3 Ma (latest Miocene-Pliocene) and implications for collision uplift. Palaeogeography, Palaeoclimatology, Palaeoecology, 331, 50-59.

32. Hantoro, W. S., Jouannic, C., & Pirazzoli, P. A. (**1989**). Terrasses coralliennes quaternaires soulevées dans l'île de Sumba (Indonésie). Photo interprétation (Paris), 28(1), 17-34.

33. Hantoro, W. S. (**1992**). Etude des terrasses récifales Quaternaires soulevées entre le Detroit de la Sonde et l'ile de Timor, Indonésie: mouvements verticaux de la croute terrestre et variations du niveau de la mer.

34. Harris, R. A. (**1991**). Temporal distribution of strain in the active Banda orogen: a reconciliation of rival hypotheses. Journal of Southeast Asian Earth Sciences, 6(3-4), 373-386.

35. Hearty, P. J., & Olson, S. L. (**2008**). Mega-highstand or megatsunami? Discussion of McMurtry et al. (Elevated marine deposits in Bermuda record a late Quaternary megatsunami: Sed. Geol. 200 (2007) 155-165). Sedimentary Geology, 203(3-4), 307-312.

36. Hein, A. S., Hulton, N. R. J., Dunai, T. J., Schnabel, C., Kaplan, M. R., Naylor, M., et al. (**2009**). Middle Pleistocene glaciation in Patagonia dated by cosmogenic-nuclide measurements on outwash gravels. Earth and Planetary Science Letters, 286(1-2), 184-197.

37. Heisinger, B., Lal, D., Jull, A. J. T., Kubik, P., Ivy-Ochs, S., Neumaier, S., et al. (**2002**). Production of selected cosmogenic radionuclides by muons: 1. Fast muons. Earth and Planetary Science Letters, 200(3-4), 345-355.

38. Hibbert, F. D., Rohling, E. J., Dutton, A., Williams, F. H., Chutcharavan, P. M., Zhao, C., et al. (**2016**). Coral indicators of past sea-level change: A global repository of U-series dated benchmarks. *Quaternary Science Reviews, 145*, 1-56.

39. Hinschberger, F., Malod, J.-A., Réhault, J.-P., Villeneuve, M., Royer, J.-Y., & Burhanuddin, S. (**2005**). Late Cenozoic geodynamic evolution of eastern Indonesia. Tectonophysics, 404(1-2), 91-118.

40. Hoeksema, B. W. (**2012**). Extreme morphological plasticity enables a free mode of life in Favia gravida at Ascension Island (South Atlantic). Marine Biodiversity, 42(2), 289-295.

41. Hopley, D. (**2011**). Density and porosity: influence on reef accretion rates. In: Springer.

42. Husson, L., Pastier, A.-M., Pedoja, K., Elliot, M., Paillard, D., Authemayou, C., et al. (**2018**). Reef carbonate productivity during Quaternary sea level oscillations. Geochemistry, Geophysics, Geosystems, pp. 1148-1164.

43. James, N. P., & Macintyre, I. G. (**1985**). Carbonate depositional environments-modern and ancient-Part. 1: Reefs-zonation, depositional facies and diagenesis. Colorado School of Mines Quarterly, 80(3).

44. Jouannic, C., Hantoro, W. S., Hoang, C. T., Fournier, M., Lafont, R., & Ichtam, M. L. (**1988**). Quaternary raised reef terraces at cape Laundi, Sumba, Indonesia: geomorphological analysis and first radiometric Th/U and 14C age determinations. Paper presented at the 6th Proceedings International coral reef symposium.

45. Kindler, P., Reyss, J.-L., Cazala, C., & Plagnes, V. r. (**2007**). Discovery of a composite reefal terrace of middle and late Pleistocene age in Great Inagua Island, Bahamas. Implications for regional tectonics and sea-level history. Sedimentary Geology, 194(1-2), 141-147.

46. Kummerow, C., Simpson, J., Thiele, O., Barnes, W., Chang, A. T. C., Stocker, E., et al. (**2000**). The status of the Tropical Rainfall Measuring Mission (TRMM) after two years in orbit. Journal of applied meteorology, 39(12), 1965-1982.

47. Lal, D. (**1988**). In situ-produced cosmogenic isotopes in terrestrial rocks. Annual Review of Earth and Planetary Sciences, 16(1), 355-388.

48. Lal, D. (**1991**). Cosmic ray labeling of erosion surfaces: in situ nuclide production rates and erosion models. Earth and Planetary Science Letters, 104(2-4), 424-439.

49. Lal, D., Gallup, C. D., Somayajulu, B. L. K., Vacher, L. c., Caffee, M. W., Jull, A. J. T., et al. (**2005**). Records of cosmogenic radionuclides 10Be, 26Al and 36Cl

in corals: First studies on coral erosion rates and potential of dating very old corals. Geochimica et cosmochimica acta, 69(24), 5717-5728.

50. Levenson, Y., Ryb, U., & Emmanuel, S. (**2017**). Comparison of field and laboratory weathering rates in carbonate rocks from an Eastern Mediterranean drainage basin. Earth and Planetary Science Letters, 465, 176-183.

51. Liew, P.-M., & Hsieh, M.-L. (**2000**). Late Holocene (2 ka) sea level, river discharge and climate interrelationship in the Taiwan region. Journal of Asian Earth Sciences, 18(4), 499-505.

52. Lundberg, J. (**2019**). Karren, surface. In Encyclopedia of Caves (pp. 600-608): Elsevier.

53. Merchel, S., Arnold, M., Aumaître, G., Benedetti, L., Bourlès, D. L., Braucher, R., et al. (**2008**). Towards more precise 10Be and 36Cl data from measurements at the 10-14 level: influence of sample preparation. Nuclear instruments and methods in physics research section B: beam interactions with materials and atoms, 266(22), 4921-4926.

54. Muhs, D. R. (**2001**). Evolution of soils on Quaternary reef terraces of Barbados, West Indies. Quaternary research, 56(1), 66-78.

55. Murray-Wallace, C. V., & Woodroffe, C. D. (**2014**). Quaternary sea-level changes: a global perspective: Cambridge University Press.

56. Nexer, M., Authemayou, C., Schildgen, T., Hantoro, W. S., Molliex, S., Delcaillau, B., et al. (**2015**). Evaluation of morphometric proxies for uplift on sequences of coral reef terraces: A case study from Sumba Island (Indonesia). Geomorphology, 241, 145-159.

57. Nugroho, H., Harris, R., Lestariya, A. W., & Maruf, B. (**2009**). Plate boundary reorganization in the active Banda Arc-continent collision: Insights from new GPS measurements. Tectonophysics, 479(1-2), 52-65.

58. Obert, J. C., Scholz, D., Felis, T., Brocas, W. M., Jochum, K. P., & Andreae, M. O. (**2016**). 230Th/U dating of Last Interglacial brain corals from Bonaire (southern Caribbean) using bulk and theca wall material. Geochimica et cosmochimica acta, 178, 20-40.

59. Obert, J. C., Scholz, D., Felis, T., Lippold, J., Jochum, K. P., & Andreae, M. O. (**2019**). Improved constraints on open-system processes in fossil reef corals by combined Th/U, Pa/U and Ra/Th dating: A case study from Aqaba, Jordan. Geochimica et cosmochimica acta, 245, 459-478.

60. Orr, Y., Schimmer, R., Geerken, R., Castro, A., Taylor, D., & Brokensha, D. (**2012**). Ethno-ecology in the shadow of rain and the light of experience: local perceptions of drought and climate change in east Sumba, Indonesia. Climate Change and Threatened Communities [Castro, AP, D. Taylor, and DW Brokensha (eds.)]. Practical Action Publishing, Rugby, UK, 175-184.

61. Pastier, A. M., Husson, L., Pedoja, K., Bézos, A., Authemayou, C., Arias-Ruiz, C., et al. (**2019**). Genesis and Architecture of Sequences of Quaternary Coral Reef Terraces: Insights From Numerical Models. Geochemistry, Geophysics, Geosystems.

62. Pedoja, K., Husson, L., Regard, V., Cobbold, P. R., Ostanciaux, E., Johnson, M. E., et al. (**2011**). Relative sea-level fall since the last interglacial stage: are coasts uplifting worldwide? Earth-Science Reviews, 108(1-2), 1-15.

63. Pedoja, K., Husson, L., Johnson, M. E., Melnick, D., Witt, C., Pochat, S. p., et al. (**2014**). Coastal staircase sequences reflecting sea-level oscillations and tectonic uplift during the Quaternary and Neogene. Earth-Science Reviews, 132, 13-38.

64. Pedoja, K., Husson, L., Bézos, A., Pastier, A.-M., Imran, A. M., Arias-Ruiz, C., et al. (**2018**). On the long-lasting sequences of coral reef terraces from SE Sulawesi (Indonesia): Distribution, formation, and global significance. Quaternary Science Reviews, 188, 37-57.

65. Phillips, F. M., & Plummer, M. A. (**1996**). CHLOE; a program for interpreting in-situ cosmogenic nuclide data for surface exposure dating and erosion studies. Radiocarbon, 38(1), 98-99.

66. Phillips, F. M., Stone, W. D., & Fabryka-Martin, J. T. (**2001**). An improved approach to calculating low-energy cosmic-ray neutron fluxes near the land/atmosphere interface. Chemical Geology, 175(3-4), 689-701.

67. Pirazzoli, P. A., Radtke, U., Hantoro, W. S., Jouannic, C., Hoang, C. T., Causse, C., et al. (**1991**). Quaternary raised coral-reef terraces on Sumba Island, Indonesia. Science, 252(5014), 1834-1836.

68. Pirazzoli, P. A., Radtke, U., Hantoro, W. S., Jouannic, C., Hoang, C. T., Causse, C., et al. (**1993**). A one million-year-long sequence of marine terraces on Sumba Island, Indonesia. Marine Geology, 109(3-4), 221-236.

69. Pirazzoli, P. A. (**2005**). A review of possible eustatic, isostatic and tectonic contributions in eight late-Holocene relative sea-level histories from the Mediterranean area. Quaternary Science Reviews, 24(18-19), 1989-2001.

70. Prasetia, R., As-syakur, A. R., & Osawa, T. (**2013**). Validation of TRMM Precipitation Radar satellite data over Indonesian region. Theoretical and applied climatology, 112(3-4), 575-587.

71. Raimbault, C., Duperret, A., Regard, V., Molliex, S., Wyns, R., Authemayou, C., et al. (**2018**). Quaternary geomorphological evolution of a granitic shore platform constrained by in situ 10Be concentrations, Penmarc'h, SW Brittany, France. Marine Geology, 395, 33-47.

72. Rasser, M., & Riegl, B. (**2002**). Holocene coral reef rubble and its binding agents. Coral Reefs, 21(1), 57-72.

73. Regard, V., Dewez, T., Bourles, D. L., Anderson, R. S., Duperret, A., Costa, S., et al. (**2012**). Late Holocene seacliff retreat recorded by 10Be profiles across a coastal platform: Theory and example from the English Channel. Quaternary Geochronology, 11, 87-97.

74. Rovere, A., Raymo, M. E., Vacchi, M., Lorscheid, T., Stocchi, P., Gomez-Pujol, L., et al. (**2016**). The analysis of Last Interglacial (MIS 5e) relative sea-level indicators: Reconstructing sea-level in a warmer world. Earth-Science Reviews, 159, 404-427.

75. Rupnik, E., Deseilligny, M. P., Delorme, A., & Klinger, Y. (**2016**). Refined satellite image orientation in the free open-source photogrammetric tools Apero/Micmac. ISPRS Annals of the Photogrammetry, Remote Sensing and Spatial Information Sciences, 3, 83.

76. Russell-Smith, J., Djoeroemana, S., Maan, J., & Pandanga, P. (**2007**). Rural livelihoods and burning practices in savanna landscapes of Nusa Tenggara Timur, eastern Indonesia. Human Ecology, 35(3), 345-359.

77. Ryb, U., Matmon, A., Erel, Y., Haviv, I., Benedetti, L., & Hidy, A. J. (**2014**). Styles and rates of long-term denudation in carbonate terrains under a Mediterranean

1145 to hyper-arid climatic gradient. Earth and Planetary Science Letters, 406, 142-
1146 152.
1147
1148 **78.** Schaller, M., Ehlers, T. A., Blum, J. D., & Kallenberg, M. A. (**2009**). Quantifying
1149 glacial moraine age, denudation, and soil mixing with cosmogenic nuclide depth
1150 profiles. Journal of Geophysical Research: Earth Surface, 114(F1).
1151
1152 **79.** Schimmelpfennig, I., Benedetti, L., Finkel, R., Pik, R. I., Blard, P.-H., Bourles,
1153 D., et al. (**2009**). Sources of in-situ 36Cl in basaltic rocks. Implications for
1154 calibration of production rates. Quaternary Geochronology, 4(6), 441-461.
1155
1156 **80.** Schimmelpfennig, I., Benedetti, L., Garreta, V., Pik, R., Blard, P.-H., Burnard,
1157 P., et al. (**2011**). Calibration of cosmogenic 36Cl production rates from Ca and
1158 K spallation in lava flows from Mt. Etna (38 N, Italy) and Payun Matru (36 S,
1159 Argentina). Geochimica et cosmochimica acta, 75(10), 2611-2632.
1160
1161 **81.** Schimmelpfennig, I., Schaefer, J. M., Putnam, A. E., Koffman, T., Benedetti, L.,
1162 Ivy-Ochs, S., et al. (**2014**). 36Cl production rate from K-spallation in the
1163 European Alps (Chironico landslide, Switzerland). Journal of Quaternary
1164 Science, 29(5), 407-413.
1165
1166 **82.** Schlagenhauf, A., Gaudemer, Y., Benedetti, L., Manighetti, I., Palumbo, L.,
1167 Schimmelpfennig, I., et al. (**2010**). Using in situ Chlorine-36 cosmonuclide to
1168 recover past earthquake histories on limestone normal fault scarps: a

reappraisal of methodology and interpretations. Geophysical Journal International, 182(1), 36-72.

83. Scholz, D., Mangini, A., & Felis, T. (**2004**). U-series dating of diagenetically altered fossil reef corals. Earth and Planetary Science Letters, 218(1-2), 163-178.

84. Schwartz, M. (**2006**). Encyclopedia of coastal science: Springer Science & Business Media.

85. Scoffin, T. P. (**1993**). The geological effects of hurricanes on coral reefs and the interpretation of storm deposits. Coral Reefs, 12(3-4), 203-221.

86. Shekeine, J., Turnbull, L. A., Cherubini, P., de Jong, R., Baxter, R., Hansen, D., et al. (**2015**). Primary productivity and its correlation with rainfall on Aldabra Atoll. Biogeosciences Discussions, 12(2), 981-1013.

87. Simms, A. R. (**2021**). Last interglacial sea levels within the Gulf of Mexico and northwestern Caribbean Sea. Earth System Science Data, 13(3), 1419-1439.

88. Smith, S. V. (**1983**). Coral reef calcification. Perspectives on Coral Reefs. Australian Institute of Marine Science, 240-247.

89. Speed, R. C., & Cheng, H. (**2004**). Evolution of marine terraces and sea level in the last interglacial, Cave Hill, Barbados. Geological Society of America Bulletin, 116(1-2), 219-232.

90. Spencer, T. (**1985**). Weathering rates on a Caribbean reef limestone: results and implications. Marine Geology, 69(1-2), 195-201.

91. Stephenson, W. J., & Kirk, R. M. (**1998**). Rates and patterns of erosion on inter-tidal shore platforms, Kaikoura Peninsula, South Island, New Zealand. Earth Surface Processes and Landforms: The Journal of the British Geomorphological Group, 23(12), 1071-1085.

92. Stone, J., Allan, G. L., Fifield, L. K., Evans, J. M., & Chivas, A. R. (**1994**). Limestone erosion measurements with cosmogenic chlorine-36 in calcite-preliminary results from Australia. Nuclear instruments and methods in physics research section B: beam interactions with materials and atoms, 92(1-4), 311-316

93. Stone, J. O., Allan, G. L., Fifield, L. K., & Cresswell, R. G. (**1996**). Cosmogenic chlorine-36 from calcium spallation. Geochimica et cosmochimica acta, 60(4), 679-692.

94. Stone, J. O. H., Evans, J. M., Fifield, L. K., Allan, G. L., & Cresswell, R. G. (**1998**). Cosmogenic chlorine-36 production in calcite by muons. Geochimica et cosmochimica acta, 62(3), 433-454.

95. Tate, G. W., McQuarrie, N., Van Hinsbergen, D. J. J., Bakker, R. R., Harris, R., Willett, S., et al. (**2014**). Resolving spatial heterogeneities in exhumation and surface uplift in Timor-Leste: Constraints on deformation processes in young orogens. Tectonics, 33(6), 1089-1112.

96. Thompson, S. B., & Creveling, J. R. (**2021**). A Global Database of Marine Isotope Stage 5a and 5c Marine Terraces and Paleoshoreline Indicators. Earth System Science Data Discussions, 1-32.

97. Trudgill, S. T. (**1976**). The marine erosion of limestones on Aldabra Atoll, Indian Ocean. Zeischrift fur Geomorphologie, 26, 164-200.

98. Trudgill, S. T. (**1979**). Surface lowering and landform evolution on Aldabra. Philosophical Transactions of the Royal Society of London. B, Biological Sciences, 286(1011), 35-45.

99. Van der Werff, W. (**1995**). Cenozoic evolution of the Savu Basin, Indonesia: forearc basin response to arc-continent collision. Marine and Petroleum Geology, 12(3), 247-262.

100. Vasconcelos, P. M. D., & Stone, J. O. (**2000**). Studies of geomorphic rates and processes with cosmogenic isotopes-examples from Australia.

101. Vermeesch, P. (**2007**). CosmoCalc: An Excel add-in for cosmogenic nuclide calculations. Geochemistry, Geophysics, Geosystems, 8(8).

102. Von Blanckenburg, F. (**2005**). The control mechanisms of erosion and weathering at basin scale from cosmogenic nuclides in river sediment. Earth and Planetary Science Letters, 242(3-4), 224-239.

103. Von der Borch, C. C., Grady, A. E., Hardjoprawiro, S., Prasetyo, H., & Hadiwisastra, S. (**1983**). Mesozoic and late Tertiary submarine fan sequences and their tectonic significance, Sumba, Indonesia. Sedimentary Geology, 37(1-2), 113-132.

104. Waelbroeck, C., Labeyrie, L., Michel, E., Duplessy, J. C., McManus, J. F., Lambeck, K., et al. (**2002**). Sea-level and deep water temperature changes derived from benthic foraminifera isotopic records. Quaternary Science Reviews, 21(1-3), 295-305.

105. Yang, Q., Scholz, D., Jochum, K. P., Hoffmann, D. L., Stoll, B., Weis, U., et al. (**2015**). Lead isotope variability in speleothems-A promising new proxy for hydrological change? First results from a stalagmite from western Germany. Chemical Geology, 396, 143-151.

Figures

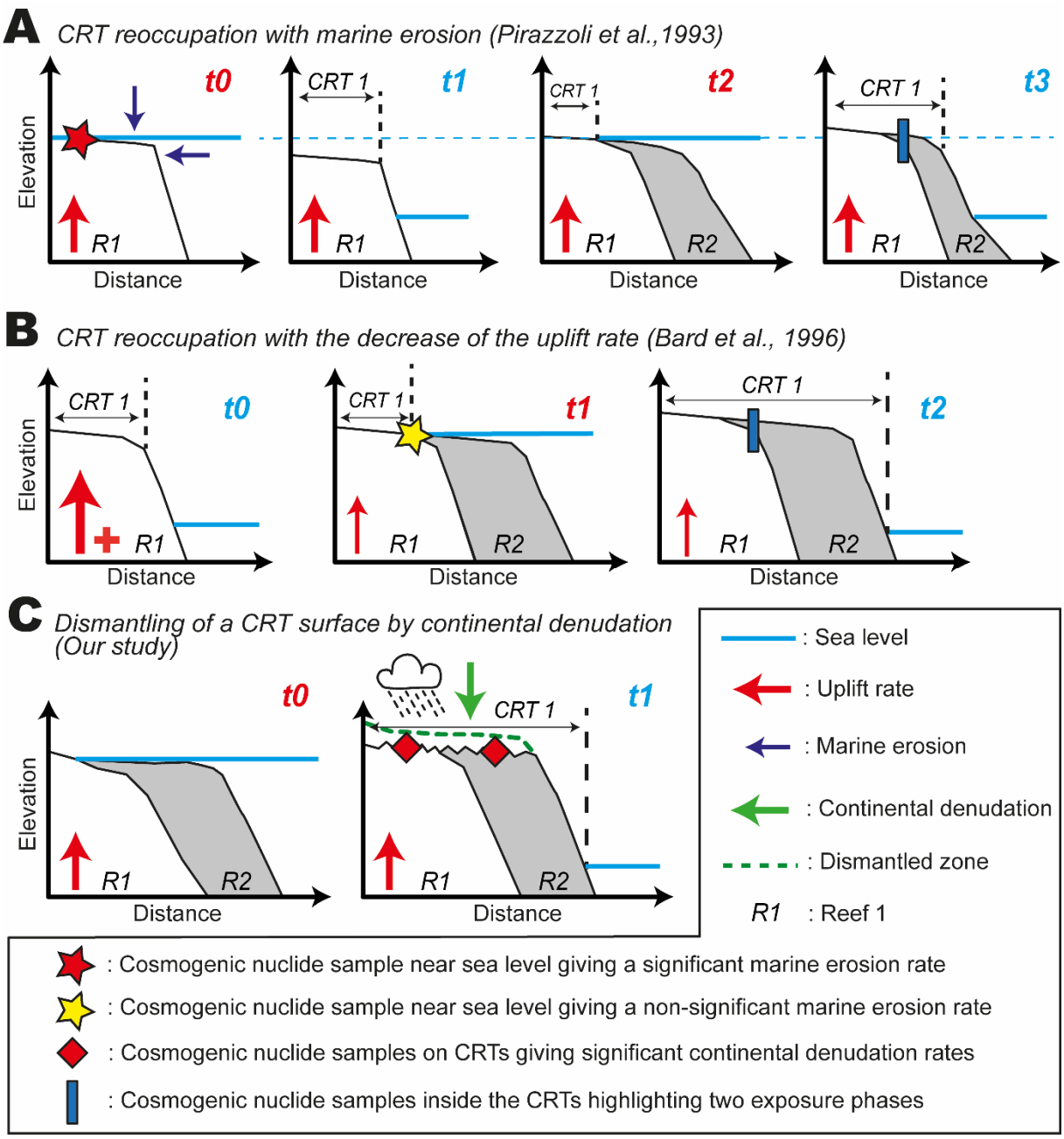
A
CRT reoccupation with marine erosion (Pirazzoli et al.,1993)
t0
t1
t2
t3
CRT 1
Elevation
R1
R2
Distance
B
CRT reoccupation with the decrease of the uplift rate (Bard et al., 1996)
C
Dismantling of a CRT surface by continental denudation (Our study)
: Sea level
: Uplift rate
: Marine erosion
: Continental denudation
: Dismantled zone
R1 : Reef 1
: Cosmogenic nuclide sample near sea level giving a significant marine erosion rate
: Cosmogenic nuclide sample near sea level giving a non-significant marine erosion rate
: Cosmogenic nuclide samples on CRTs giving significant continental denudation rates
: Cosmogenic nuclide samples inside the CRTs highlighting two exposure phases

Fig. 1. Three hypotheses explaining diachronous ages on the same surface of the Cape Laundi CRTs. **A) I**mportant role of marine erosion in the destruction of the emergent CRTs, helping a later reoccupation of these eroded surfaces (Pirazzoli et al., 1993). **B)** The decrease in the rate of uplift to a low rate (about 0.2 mm a^{-1}) promotes the reoccupation of emergent CRTs whitout marine erosion (Bard et al., 1996). **C)** Alternative hypothesis (this study): continental denudation may partially dismantle emergent surfaces, generating a diachronism of these surfaces. ^{36}Cl cosmonuclides data on CRT near current sea level reveal the significance of marine erosion (Fig. 1A) and continental denudation (Fig. 1C).

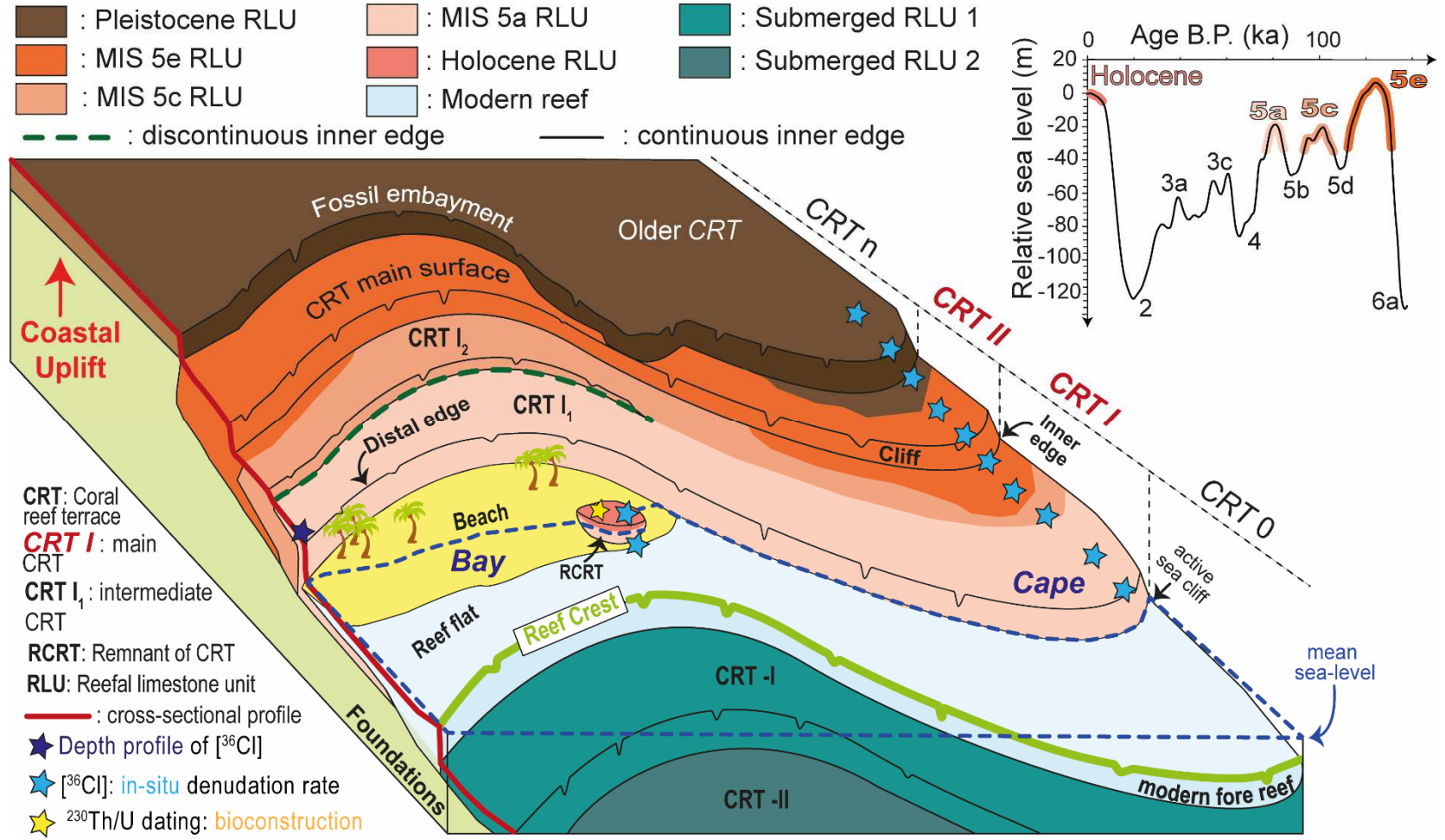

1276 **Fig. 2.** Schematic plot of a sequence of coral reef terraces, modified from Pedoja et al. (2018). The blue and yellow stars represent

1277 the location of samples collected on the CRT surfaces and intended for analysis in ^{36}Cl concentration and $^{230}Th/U$ dating, respectively.

1278 The relative sea level curve is from Waelbroeck et al. (2002).

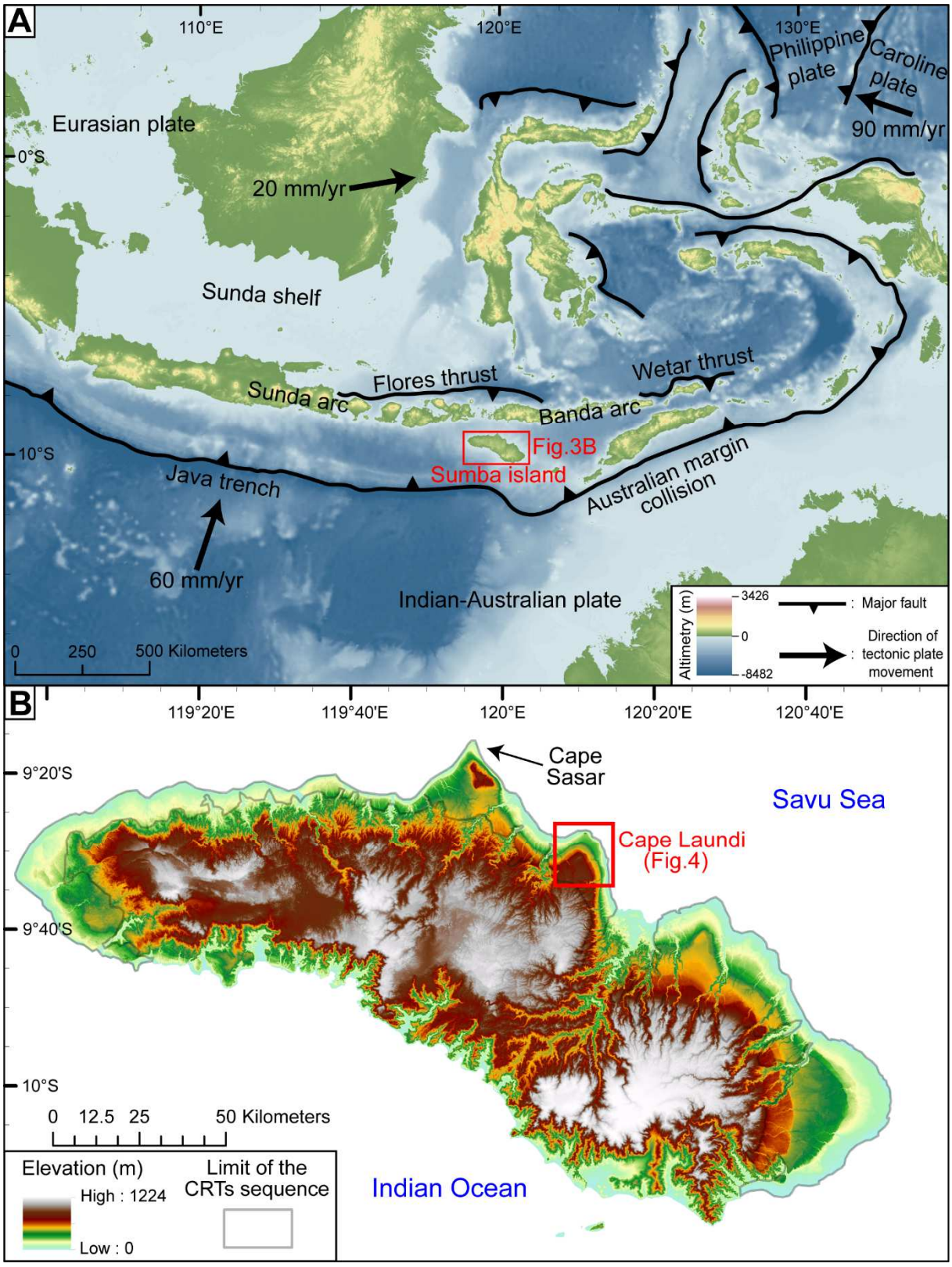

Fig. 3. A) Geodynamics of SE Asia and location of Sumba Island (Indonesia). Plate velocities indicated in relation to the Eurasia plate, from Nugroho et al. (2009), elevation data from the Shuttle Radar Topography Mission (SRTM), and bathymetry

data from the General Bathymetric Chart of Oceans (GEBCO), both at 90 m resolution. **B)** Digital elevation model (TanDEM-X, 13 m resolution) of Sumba Island.

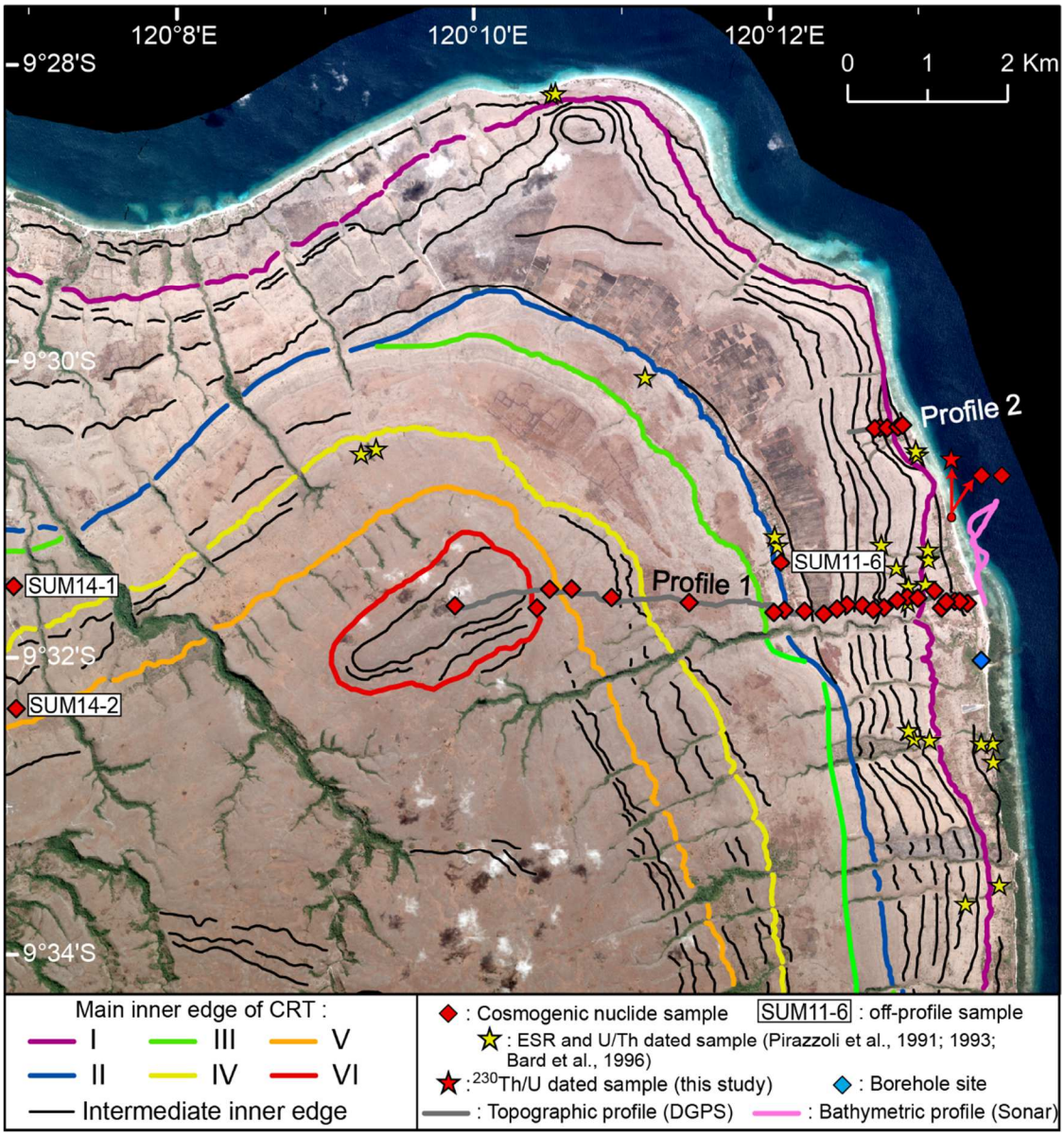

1285 **Fig. 4.** CRTs inner edges of the Cape Laundi sequence (Pleiades satellite imagery, 1

1286 m resolution), and the location of samples, topographic and bathymetric profiles.

1287

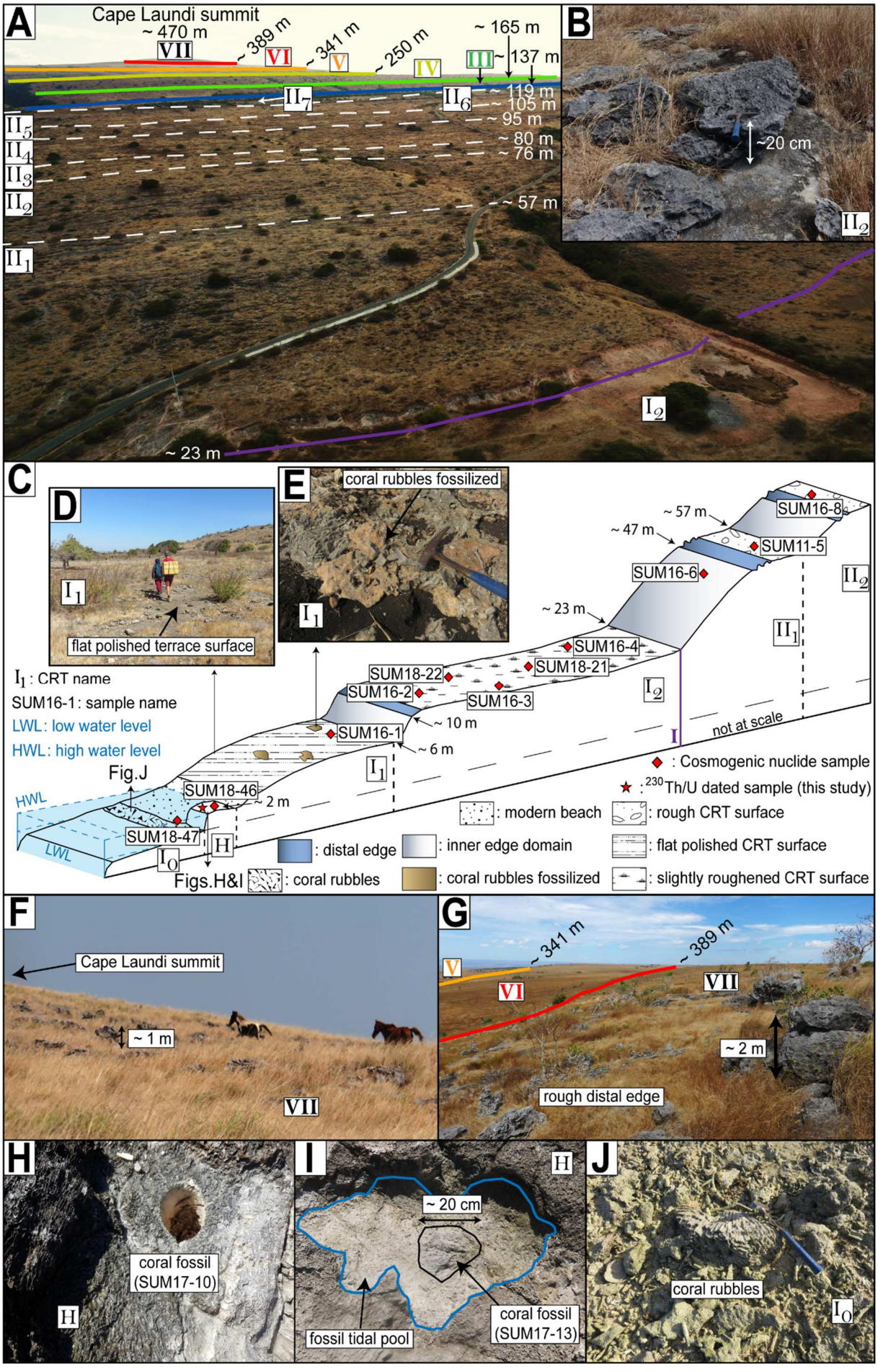
A
Cape Laundi summit
~ 470 m
~ 389 m
~ 341 m
~ 250 m
~ 165 m
~ 137 m
~ 119 m
~ 105 m
~ 95 m
~ 80 m
~ 76 m
~ 57 m
~ 23 m
B
~20 cm
C
D
flat polished terrace surface
E
coral rubbles fossilized
~ 57 m
~ 47 m
~ 23 m
~ 10 m
~ 6 m
~ 2 m
SUM16-8
SUM11-5
SUM16-6
SUM16-4
SUM18-21
SUM18-22
SUM16-2
SUM16-3
SUM16-1
SUM18-46
SUM18-47
HWL
LWL
Fig.J
Figs.H&I
not at scale
I1 : CRT name
SUM16-1: sample name
LWL: low water level
HWL: high water level
: Cosmogenic nuclide sample
: 230Th/U dated sample (this study)
: modern beach
: rough CRT surface
: distal edge
: inner edge domain
: flat polished CRT surface
: coral rubbles
: coral rubbles fossilized
: slightly roughened CRT surface
F
Cape Laundi summit
~ 1 m
G
~ 341 m
~ 389 m
~ 2 m
rough distal edge
H
coral fossil
(SUM17-10)
I
~ 20 cm
fossil tidal pool
coral fossil
(SUM17-13)
J
coral rubbles

Fig. 5. Pictures and interpretations of the Cap Laundi CRTs sequence. The elevations result from the DGPS profile. **A)** Aerial photo of Cape Laundi showing the staircase coastal landscape. **B)** CRT II_2 surface. **C)** Schematic 3D diagram of the lowest CRTs, with locations of Figs. 5D; 5E; 5H; 5I; 5J. **D)** Smooth flat surface of CRT I_1. **E)** Fossil coral rubbles cemented within the reefal limestones outcropping on the CRT I_1 surface. **F)** Cape Laundi summit. **G)** Distal edge of CRT VII. **H)** Sample SUM17-10. **I)** Sample SUM17-13). **J)** Coral rubbles on the modern reef flat (CRT I_0).

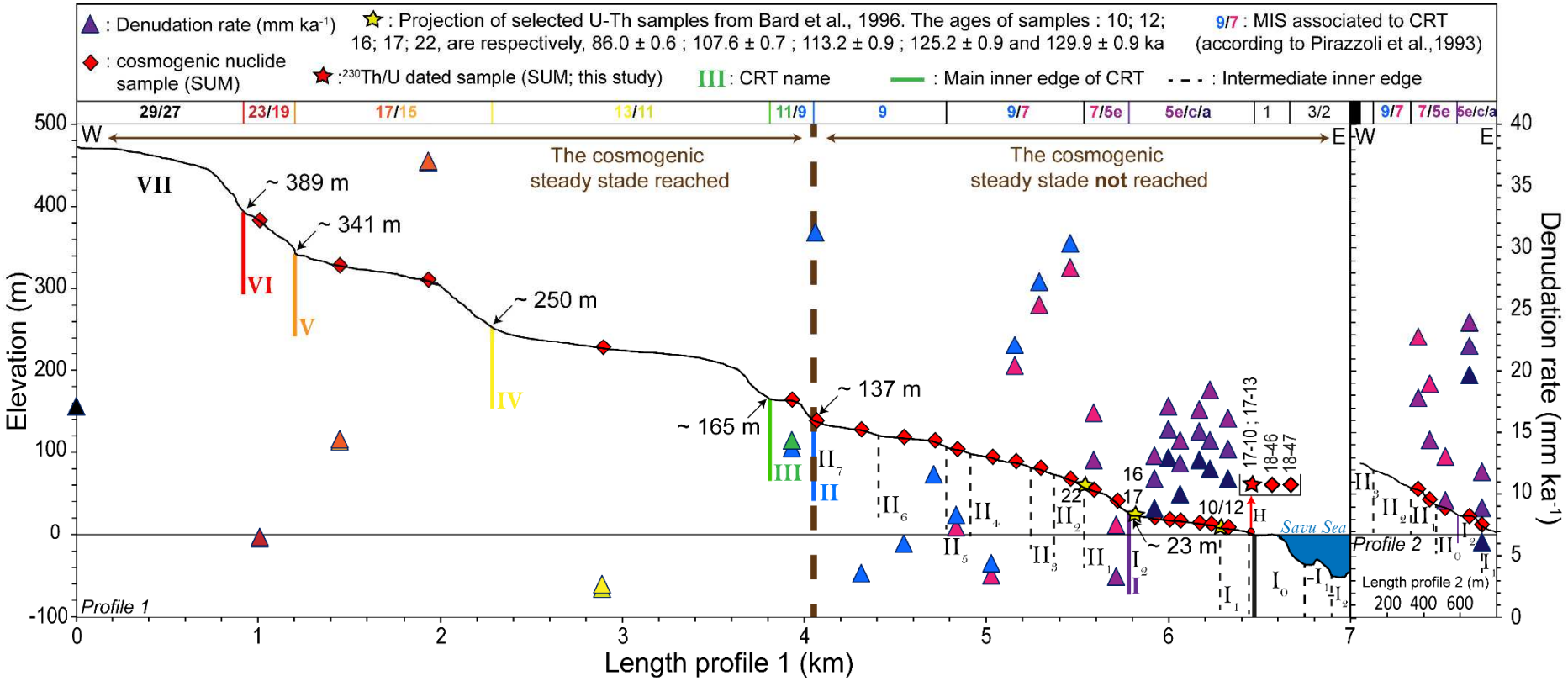

1295 **Fig. 6.** Altimetric profiles (DGPS and sonar) at Cape Laundi, showing the calculated denudation rates with various age hypotheses

1296 (the colors of the triangles correspond to different age hypotheses), as well as location and ages of U/Th samples (Bard et al., 1996;

1297 this study).

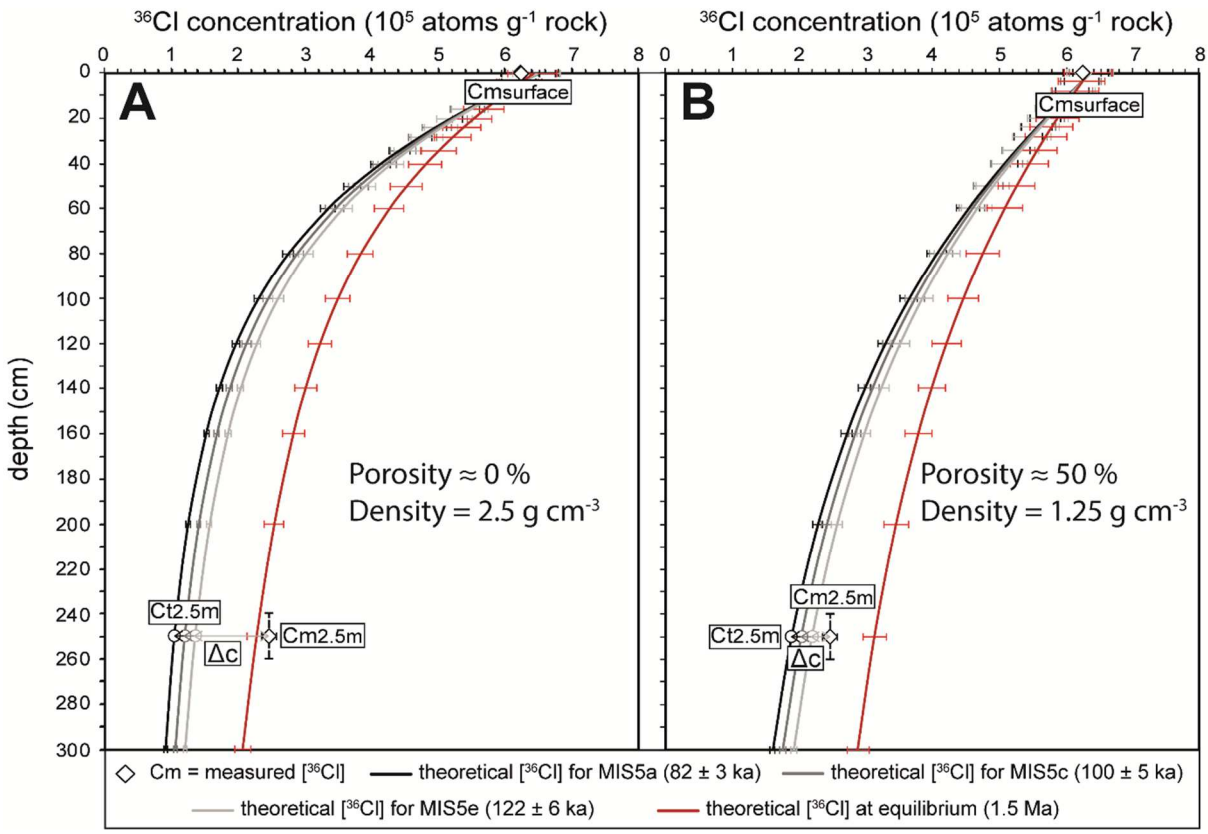

1298 **Fig. 7.** Surface (Cmsurface) and 2.5 ± 0.1 m (Cm2.5m) depth ^{36}Cl concentration of the
1299 borehole within CRT I_1 for a porosity of **A)** 50 % (i.e., density = 1.25 g cm^{-3}) and **B)** 0%
1300 (density = 2.5 g cm^{-3}). Theoretical ^{36}Cl concentration curves as a function of depth and
1301 MIS and age hypotheses. Δc is the difference between measured ^{36}Cl (Cm2.5m) and
1302 theorical concentrations at 2.5 ± 0.1 m depth (Ct2.5m).

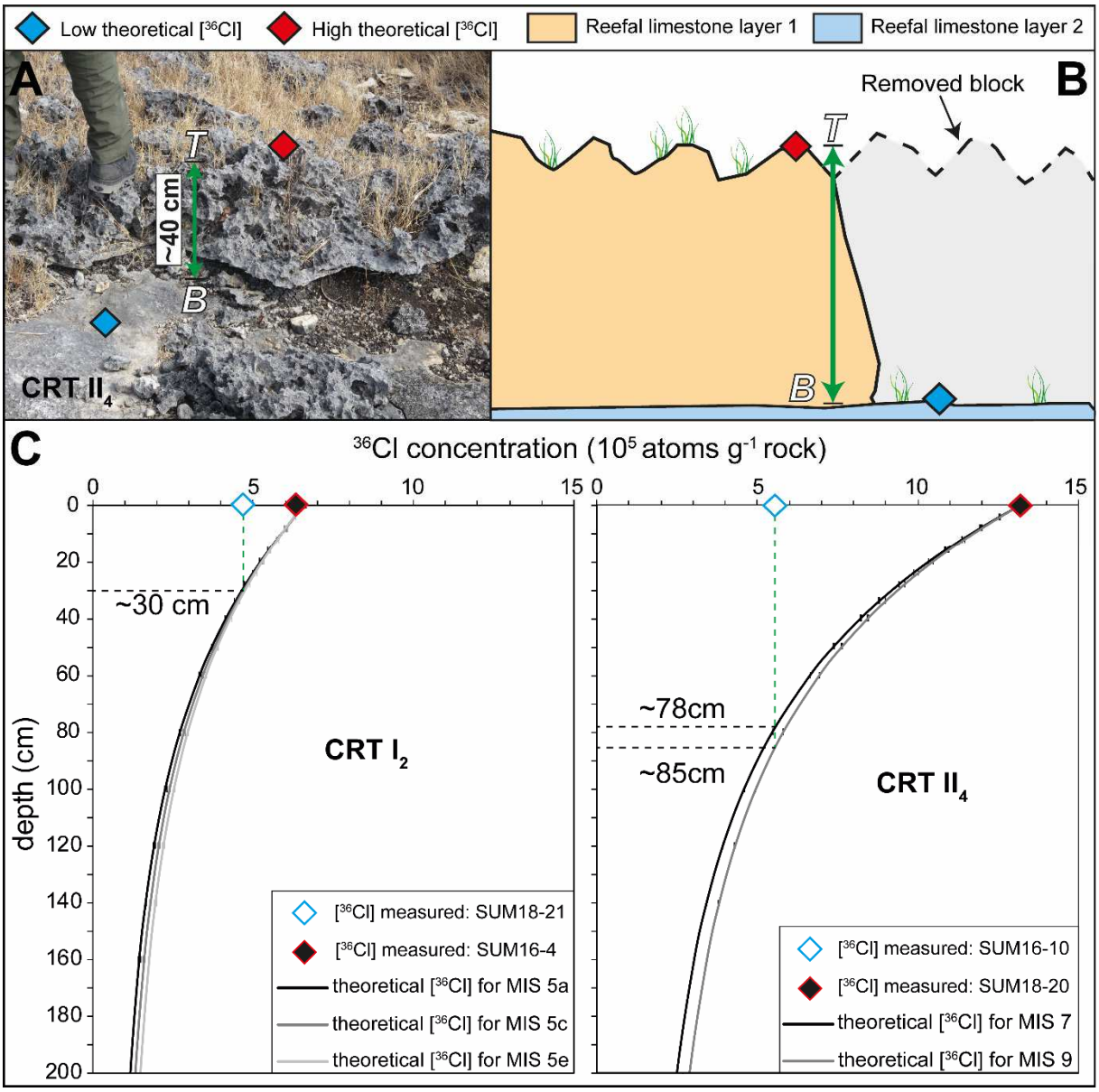

Fig. 8. ^{36}Cl concentration variations at the scale of a CRT. **A)** Epikarstification on the surface of CRT II_4. **B)** Schematic cross-sectional view of Figure 7A. *T* and *B* correspond to the top and bottom of the reefal limestone layer 1, respectively. **C)** Theoretical ^{36}Cl concentration curves of depth for 2 samples pairs (SUM18-21/16-4 and SUM18-20/16-10) as a function of depth and MIS and age hypotheses, assuming that the ages of reefal bioconstruction and exposure duration are synchronous, as proposed by Pirazzoli et al. (1991; 1993).

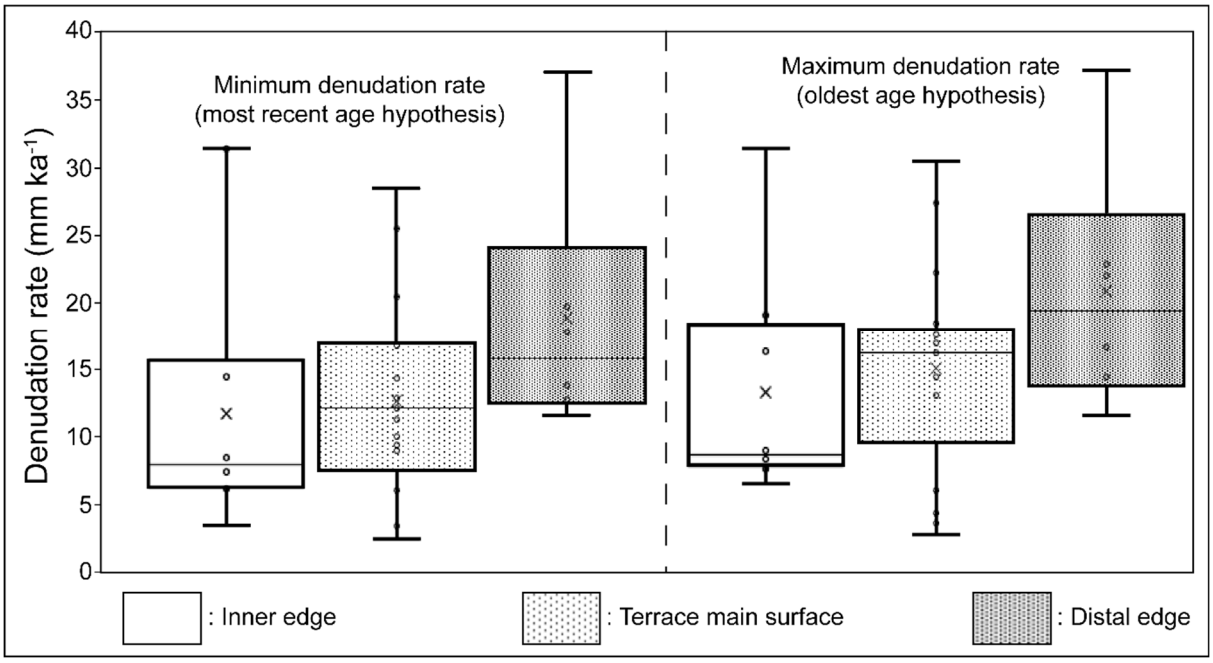

Fig. 9. Boxplots of denudation rates, calculated with the most recent and oldest age hypothesis, classified by morphological zone. The crosses, inner bars, circles, upper, and lower outer bars represent the average, median, data, maximum and minimum value for ^{36}Cl concentrations, respectively.

Tables

Sample (SUM)	Sample information						Sample composition		^{230}Th/U chemistry							
	Coral species	CRT	Morphology location	Longitude (E)	Latitude (N)	Elevation (m)	Calcite (%)	Aragonite (%)	^{238}U (µg/g)	^{232}Th (ng/g)	(^{234}U/^{238}U)	(^{230}Th/^{238}U)	age uncorrected (ka)	age corrected (ka)	MIS	(^{234}U/^{238}U)initial
17-10	*Pseudodiploria clivosa*	H	Distal edge	120.221	-9.52	2.0 ± 0.5	< 1	> 99	2.37 ± 0.01	1.080 ± 0.006	1.14627 ± 0.00041	0.05584 ± 0.00020	5.460 ± 0.020	5.448 ± 0.02	1	1.14854 ± 0.00040
17-13	*Mussismilia leptophylla*	H	Distal edge	120.221	-9.52	2.0 ± 0.5	< 1	> 99	3.02 ± 0.02	1.281 ± 0.007	1.1404 ± 0.0003	0.02199 ± 0.00010	2.1359 ± 0.0083	2.1252 ± 0.0098	1	1.14126 ± 0.00030

Table 1. Results of ^{230}Th/U dating of samples SUM17-10 and SUM17-13.

Sample (SUM)	Sample location, elevation, slope and Mean Annual Precipitation (MAP)							Sample composition			AMS result
	DGPS profile	CRT name	Longitude (E)	Latitude (N)	Elevation (m)	Slope (°)	MAP (mm yr^{-1})	Cl (target fraction) (ppm ± 0.12)	CaO (target fraction) (wt% ± 0.25)	MgO (bulk rock) (wt%)	[^{36}Cl] (10^5 atom g^{-1} rock)
16-1	Profile 1	I1	120.2222	-9.5272	8.4 ± 0.5	0.0	722.8	26.23	55.24	0.39	5.95 ± 0.14
16-2	Profile 1	I2	120.2213	-9.5270	12.5 ± 0.5	2.6	722.3	15.08	54.82	0.47	5.43 ± 0.13
18-22	Profile 1	I2	120.2208	-9.5270	14.4 ± 0.5	1.5	723.3	14.17	52.06	0.57	4.82 ± 0.11
16-3	Profile 1	I2	120.2198	-9.5271	17.4 ± 0.5	3.8	727.3	12.26	56.61	0.36	6.1 ± 0.14
18-21	Profile 1	I2	120.2193	-9.5278	18.5 ± 0.5	1.5	739.9	6.29	54.34	0.32	4.69 ± 0.10
16-4	Profile 1	I2	120.2185	-9.5258	20.4 ± 0.5	1.7	723.9	14.94	55.77	0.29	6.26 ± 0.14
16-6	Profile 1	II1	120.2166	-9.5266	40.7 ± 0.5	14.9	750.7	3.07	55.80	0.34	9.7 ± 0.22
11-5	Profile 1	II1	120.2154	-9.5266	54.4 ± 0.5	4.2	760.1	18.97	53.62	0.68	6.33 ± 0.14
16-8	Profile 1	II2	120.2143	-9.5269	67.5 ± 0.5	4.5	774.6	6.49	55.51	0.47	4.45 ± 0.10
16-9	Profile 1	II3	120.2128	-9.5277	80.2 ± 0.5	4.0	797.7	8.81	55.37	0.31	4.8 ± 0.11
16-10	Profile 1	II4	120.2116	-9.5279	88.1 ± 0.5	3.1	811.6	2.89	55.14	0.15	5.53 ± 0.12
18-20	Profile 1	II4	120.2104	-9.5275	94.4 ± 0.5	3.6	816.7	1.75	52.58	0.40	13.17 ± 0.31
18-19	Profile 1	II5	120.2086	-9.5274	104.0 ± 0.5	3.3	831.3	3.67	53.59	0.28	9.54 ± 0.19
18-18	Profile 1	II6	120.2075	-9.5279	113.9 ± 0.5	3.6	847.2	2.47	52.72	0.36	7.63 ± 0.17
18-17	Profile 1	II6	120.2060	-9.5284	117.9 ± 0.5	1.5	867.0	4.32	52.75	0.34	11.47 ± 0.23
18-16	Profile 1	II7	120.2039	-9.5281	127.8 ± 0.5	3.6	881.6	5.57	47.47	0.42	13.57 ± 0.26
18-15	Profile 1	II7	120.2016	-9.5280	138.6 ± 0.5	8.2	901.0	3.16	50.46	0.30	3.80 ± 0.08
18-14	Profile 1	III	120.2004	-9.5283	163.0 ± 0.5	6.0	913.9	2.16	54.33	0.24	7.20 ± 0.16
18-37	Profile 1	IV	120.1909	-9.5272	227.1 ± 0.5	6.2	987.1	4.42	51.70		20.00 ± 0.37
18-36	Profile 1	V	120.1822	-9.5266	309.5 ± 1.5	7.3	1059.6	2.87	52.19	0.20	4.04 ± 0.09
18-35	Profile 1	V	120.1777	-9.5256	327.2 ± 1.5	8.8	1073.7	2.23	53.19	0.25	8.50 ± 0.17
18-31	Profile 1	VI	120.1738	-9.5278	380.5 ± 1.5	3.5	1101.7	2.43	53.20	0.46	15.00 ± 0.28
18-33	Profile 1	VII	120.1646	-9.5275	471.6 ± 1.5	2.7	1109.8	4.06	51.42	0.20	8.01 ± 0.17
18-24	Profile 2	I1	120.2149	-9.5072	14.7 ± 0.5	14.4	765.6	38.37	52.12	0.51	7.26 ± 0.16
18-25	Profile 2	I2	120.2144	-9.5074	25.8 ± 0.5	3.1	767.4	7.37	52.29	0.29	3.68 ± 0.08
18-26	Profile 2	II0	120.2132	-9.5075	35.2 ± 0.5	7.0	774.4	49.08	51.88	0.63	8.31 ± 0.21
18-28	Profile 2	II1	120.2123	-9.5075	43.3 ± 0.5	10.6	779.6	3.96	53.32	0.50	5.11 ± 0.11
18-27	Profile 2	II1	120.2118	-9.5076	56.1 ± 0.5	12.1	782.4	9.24	51.62	0.29	5.11 ± 0.11
Cm$_{surface}$	Borehole	I1	120.2237	-9.5336	2.8 ± 0.5	0.0	790.6	12.26	56.61	0.36	6.23 ± 0.14
Cm$_{2.5m}$	Borehole	I1	120.2237	-9.5336	-2.5 ± 0.1			18.15	52.49	0.75	2.46 ± 0.06
18-46	Off profile	I1	120.2207	-9.5179	2.0 ± 0.5	0.0	638.9	245.15	47.14	2.67	0.38 ± 0.04
18-47	Off profile	I0	120.2207	-9.5179	0.0	0.0	638.9	178.84	49.93	1.43	0.30 ± 0.03
11-6	Off profile	II6	120.2009	-9.5217	149.3 ± 0.5	2.1	830.8	3.38	55.33	0.38	10.82 ± 0.23
14-2	Off profile	IV	120.1139	-9.5274	210.8 ± 0.5	3.5	1094.4	2.22	55.33	0.26	7.07 ± 0.15
14-2	Off profile	V	120.1141	-9.5407	293.9 ± 1.5	3.4	1142.8	1.97	55.69	0.14	8.27 ± 0.18

Table 2. Bedrock sample information, location, elevation, chemical composition, and AMS ^{36}Cl results. Mean annual precipitation (MAP) values are TRMM data (e.g., Kummerow et al., 2000).

Sample (SUM)	Morphology location	AMS result [^{36}Cl] (10^5 atom g-1)	Hypothesis 1			Hypothesis 2			Hypothesis 3			Mean denudation rate	Integration time
			MIS	Exposure duration (ka)	Denudation rate (mm ka^{-1})	MIS	Exposure duration (ka)	Denudation rate (mm ka^{-1})	MIS	Exposure duration (ka)	Denudation rate (mm ka^{-1})	(mm ka^{-1})	(ka)
16-1	Terrace main surface	5.95 ± 0.14	5a	82 ± 3	11.3 ± 0.1	5c	100 ± 5	13.7 ± 0.1	5e	122 ± 6	16.2 ± 0.1	13.7 ± 2.5	44.7 ± 8.0
16-2	Terrace main surface	5.43 ± 0.13	5a	82 ± 3	12.1 ± 0.1	5c	100 ± 5	14.4 ± 0.1	5e	122 ± 6	18.4 ± 0.1	15.0 ± 3.2	41.2 ± 8.5
18-22	Terrace main surface	4.82 ± 0.11	5a	82 ± 3	12.8 ± 0.4	5c	100 ± 5	175.1 ± 0.4	5e	122 ± 6	16.9 ± 0.4	14.9 ± 2.1	40.7 ± 5.7
16-3	Terrace main surface	6.1 ± 0.14	5a	82 ± 3	10.0 ± 0.1	5c	100 ± 5	12.5 ± 0.1	5e	122 ± 6	14.4 ± 0.1	12.3 ± 2.2	49.9 ± 9.3
18-21	Terrace main surface	4.69 ± 0.10	5a	82 ± 3	13.0± 0.4	5c	100 ± 5	15.2 ± 0.4	5e	122 ± 6	17.1 ± 0.4	15.1 ± 2.1	40.3 ± 5.7
16-4	Terrace main surface	6.26 ± 0.14	5a	82 ± 3	8.9 ± 0.1	5c	100 ± 5	11.3 ± 0.1	5e	122 ± 6	13.1 ± 0.1	11.1 ± 2.1	55.5 ± 11.3
16-6	Inner edge	9.7 ± 0.22	5e	122 ± 6	3.4 ± 0.0(2)	7e	239.5 ± 8.5	7.6 ± 0.0(2)				5.5 ± 2.9	127.9 ± 68.6
11-5	Distal edge	6.33 ± 0.14	5e	122 ± 6	12.8 ± 0.1	7e	239.5 ± 8.5	16.7 ± 0.1				14.7 ± 2.8	41.6 ± 7.8
16-8	Terrace main surface	4.45 ± 0.10	7e	239.5 ± 8.5	28.4 ± 0.2	9e	325 ± 18.5	30.4 ± 0.2				29.4 ± 1.4	20.4 ± 1.0
16-9	Terrace main surface	4.8 ± 0.11	7e	239.5 ± 8.5	25.4 ± 0.2	9e	325 ± 18.5	27.3 ± 0.2				26.4 ± 1.3	22.8 ± 1.1
16-10	Terrace main surface	5.53 ± 0.12	7e	239.5 ± 8.5	20.4 ± 0.1	9e	325 ± 18.5	22.1 ± 0.1				21.3 ± 1.2	28.3 ± 1.6
18-20	Terrace main surface	13.17 ± 0.31	7e	239.5 ± 8.5	3.4 ± 0.1	9e	325 ± 18.5	4.4 ± 0.1				3.9 ± 0.7	156.0 ± 26.8
18-19	Inner edge	9.54 ± 0.19	7e	239.5 ± 8.5	7.4 ± 0.2	9e	325 ± 18.5	8.3 ± 0.2				7.8 ± 0.7	76.8 ± 6.4
18-18	Distal edge	7.63 ± 0.17	9e	325 ± 18.5	11.6 ± 0.3							11.6 ± 0.3	51.7 ± 0.1
18-17	Terrace main surface	11.47 ± 0.23	9e	325 ± 18.5	6.0 ± 0.1							6.0 ± 0.1	99.5 ± 0.1
18-16	Terrace main surface	13.57 ± 0.26	9e	325 ± 18.5	3.6 ± 0.1							3.6 ± 0.1	164.8 ± 0.1
18-15	Inner edge	3.80 ± 0.08	9e	325 ± 18.5	31.3 ± 0.8							31.3 ± 0.8	19.2 ± 0.1
18-14	Distal edge	7.20 ± 0.16	9e	325 ± 18.5	13.8 ± 0.4	11c	390 ± 30	14.4 ± 0.4				14.1 ± 0.4	42.5 ± 1.4
18-37	Terrace main surface	20.00 ± 0.37	11c	390 ± 30	2.3 ± 0.1	13a	495 ± 15	2.8 ± 0.1				2.5 ± 0.3	237.3 ± 27.0
18-36	Distal edge	4.04 ± 0.09	15e	610 ± 10	37.0 ± 0.9	17c	695 ± 15	37.1 ± 0.9				37.1 ± 0.1	16.2 ± 0.3
18-35	Terrace main surface	8.50 ± 0.17	15e	610 ± 10	14.3 ± 0.3	17c	685 ± 15	14.4 ± 0.3				14.4 ± 0.1	41.8 ± 0.3
18-31	Inner edge	15.00 ± 0.28	19	780 ± 10	6.4 ± 0.1	21	850 ± 15	6.5 ± 0.1	23	910 ± 10	6.6 ± 0.1	6.5 ± 0.1	92.4 ± 0.8
18-33	Terrace main surface	8.01 ± 0.17	27	980 ± 5	17.1 ± 0.4	29	1020 ± 10	17.2 ± 0.4				17.2 ± 0.0(1)	35.0 ± 0.1
18-24	Inner edge	7.26 ± 0.16	5a	82 ± 3	6.1 ± 0.2	5c	100 ± 5	8.9 ± 0.2	5e	122 ± 6	10.8 ± 0.2	8.6 ± 2.4	73.8 ± 22.1
18-25	Distal edge	3.68 ± 0.08	5a	82 ± 3	19.7 ± 0.5	5c	100 ± 5	22.0 ± 0.5	5e	122 ± 6	24.0 ± 0.2	21.9 ± 2.2	27.6 ± 2.8
18-26	Terrace main surface	8.31 ± 0.21	5e	122 ± 6	9.4 ± 0.2	7e	239.5 ± 8.5	13.0 ± 0.2				11.2 ± 2.6	55.1 ± 12.8
18-28	Inner edge	5.11 ± 0.11	5e	122 ± 6	14.4 ± 0.4	7e	239.5 ± 8.5	19.0 ± 0.4				16.7 ± 3.3	36.6 ± 7.1
18-27	Distal edge	5.11 ± 0.11	5e	122 ± 6	17.8 ± 0.5	7e	239.5 ± 8.5	22.8 ± 0.5				20.3 ± 3.5	30.0 ± 5.3
18-46	Distal edge	0.38 ± 0.04	Holocene	2.13 ± 0.01	279.0 ± 0.4	Holocene	5.45 ± 0.02	581.0 ± 0.4				430 ± 214	1.6 ± 2.8
11-6	Inner edge	10.82 ± 0.23	9e	325 ± 18.5	8.4 ± 0.2							8.4 ± 0.2	71.4 ± 0.1
14-1	Terrace main surface	7.07 ± 0.15	11c	390 ± 30	16.8 ± 0.4	13a	495 ± 15	17.5 ± 0.4				17.1 ± 0.5	35.0 ± 1.1
14-2	Inner edge	8.27 ± 0.18	15e	610 ± 10	16.1 ± 0.4	17c	685 ± 15	16.3 ± 0.4				16.2 ± 0.1	37.0 ± 0.3

1332

Table 3. Morphology location and calculated denudation rates from the ^{36}Cl concentrations and the different MIS and age hypotheses, assuming that the ages of reefal bioconstruction and exposure duration are synchronous, for each CRT of the sequence as proposed by Pirazzoli et al. (1991; 1993). The MIS ages and their uncertainties are derived from Cutler et al. (2003) and Murray-Wallace and Woodroffe (2014). Denudation rate uncertainties are calculated by standard error propagation, including uncertainties from production rates, ages, and AMS measurements. Mean denudation rate uncertainties are calculated using the standard deviation.

Porosity	Density	Ed		Denudation rate	Ct2.5m	Δc	EdΔc
%	(g cm^{-3})	MIS	ka	(mm ka^{-1})	(10^5 atoms g $rock^{-1}$)	(10^5 atoms g $rock^{-1}$)	ka
50	1.25	5a	82 ± 3	20.0 ± 0.2	1.88 ± 0.03	0.58 ± 0.15	5.4 ± 1.3
		5c	100 ± 5	24.9 ± 0.2	2.02 ± 0.03	0.44 ± 0.15	4.0 ± 1.2
		5e	122 ± 6	28.6 ± 0.3	2.18 ± 0.03	0.28 ± 0.15	2.6 ± 1.2
0	2.5	5a	82 ± 3	9.5 ± 0.2	1.05 ± 0.03	1.41 ± 0.15	13.8 ± 1.3
		5c	100 ± 5	11.9 ± 0.2	1.19 ± 0.03	1.27 ± 0.15	12.5 ± 1.2
		5e	122 ± 6	13.8 ± 0.3	1.34 ± 0.03	1.15 ± 0.15	11.0 ± 1.2

Table 4. Borehole ^{36}Cl theoretical concentrations and theoretical exposure duration within CRT I_1. Ed, MIS, Ct2.5m, Δc, EdΔc, correspond to the exposure duration for surface sample (Cmsurface), Marine Isotope Stage, ^{36}Cl theoretical concentration at 2.5 ± 0.1 m depth (Ct2.5m) calculated from the ^{36}Cl measured concentration of the surface sample, the difference between ^{36}Cl measured (Cm2.5m) and theoretical concentrations at 2.5 ± 0.1 m depth (Ct2.5m), the theoretical exposure duration calculated from Δc, respectively. The ages and their uncertainties are derived from Cutler et al. (2003) and Murray-Wallace and Woodroffe (2014).